IEEE Access
Multidisciplinary | Rapid Review | Open Access Journal

Received May 25, 2019, accepted June 20, 2019, date of publication June 24, 2019, date of current version July 22, 2019.

Digital Object Identifier 10.1109/ACCESS.2019.2924873

Robust Control of Air-Breathing Hypersonic Vehicles With Adaptive Projection-Based Parameter Estimation

SHILI TAN, JIONG LI, AND HUMIN LEI
Air and Missile Defense College, Air Force Engineering University, Xi'an 710051, China

Corresponding authors: Shili Tan (tanslchn@163.com) and Jiong Li (graceful001@163.com)

This work was supported in part by the National Natural Science Foundation of China under Grant 61603410, Grant 61703421, Grant 61773398, and Grant 61873278.

ABSTRACT A robust controller with an adaptive projection-based parameter estimator is presented for the air-breathing hypersonic vehicles. First, a novel parameter-varying model is established wherein the number of variable parameters is significantly reduced. In this way, the problem of overparameterization is avoided, and the controller design procedure is simplified. Then, the framework of the controller is established based on the backstepping approach, in which a second-order filter is introduced to solve the problem of ''explosion of terms''. In order to enhance the robustness of the controller, an adaptive parameter estimator is designed. The Lipschitz continuous dead-zone modification is used to solve the problem of parameter draft in the conventional adaptive control and a sufficiently smooth projection operator is introduced to guarantee the uniform boundedness of adaptive parameters. The simulation results show that the proposed robust controller achieves the stable tracking of the reference commands under the parameter perturbation, and the variable parameters are limited within the preset range.

INDEX TERMS Air-breathing hypersonic vehicle, robust control, adaptive control, parameter estimation, projection operator.

I. INTRODUCTION

The air-breathing hypersonic vehicle (AHV) powered by scramjet has attracted tremendous attention for its cost-effective access to space and great potential for prompt global reaching capability [1]. The model of AHV is highly complex due to the variable flight conditions, strong nonlinearity, inherent aero-propulsive coupling, structural elasticity, and parameter perturbation [2]. Therefore, the controller design for AHV is a huge challenge.

Recently, researchers have been paying much attention to the design of the flight control system for AHV. An improved nonlinear dynamic inversion is presented for the longitudinal dynamics of AHV wherein the optimal feedback gain is determined by the genetic algorithm and the pole placement technique [3]. To deal with the nonlinearity of AHV model, the backstepping is widely used as an effective control approach. A dynamic surface control technique, in which a first-order filter is inserted to obtain the derivatives of the designed virtual control inputs, is adopted in [4]. By the above-mentioned methods, the problem of ''explosion of terms'' in the conventional backstepping is avoided. In order to further simplify the design procedure and the backstepping control scheme, an improved backstepping design approach is presented to avoid the problem of repeated differentiation [5]. Using the above simplified backstepping approach, Wu *et al.* designed an adaptive robust controller for the output tracking of a strict-feedback system with time-varying delays [6]. In addition, a controller based on the radial basis function neural network (RBFNN), without backstepping, is designed [7]. As for the adaptive updating of the RBFNN weights, a composite learning law with the novel prediction error is proposed. Moreover, the high order sliding mode (HOSM) control, as well as the input-output linearization, are used for output tracking control of AHV [8]. The above researches were carried out on the basis of an affine model. However, the model of AHV lost some of its dynamic characteristics in the process of conversion to

The associate editor coordinating the review of this manuscript and approving it for publication was Yanzheng Zhu.

an affine model, which is unfavorable for the precise control. Some researchers have made positive contributions on designing controllers directly based on the non-affine model. Chen *et al.* analyzed the effects of non-affine terms on the altitude dynamics and designed a non-affine controller combining the sliding mode control and the Takagi-Sugeno (T-S) fuzzy method. Bu *et al.* designed the non-affine controller with a simple structure by introducing the improved backstepping approach, in which the RBFNN is used to estimate the total uncertainty dynamics [10]. Furthermore, a prescribed performance control strategy, based on the non-affine model, is proposed for AHV, ensuring the tracking errors within a prescribed performance [11].

Robustness is a basic requirement for the designed controller and is directly related to the achievement of control target. Typical robust control methods include H_∞, μ-synthesis, and robust adaptive control. Firstly, the H_∞ control approach is reviewed. A self-scheduled decoupling control is presented in [12], in which the decoupling problem is transformed to the robust H_∞ control problem of a general linear parameter-varying (LPV) error system. It is noted that the H_∞ control is defined under the assumption that the energy of disturbances is finite. However, the practical disturbances are persistent, which do not satisfy the assumption of the H_∞ control. Thus, Wu *et al*. designed a robust controller with a guaranteed L_∞-gain performance of disturbances wherein a L_∞-gain control is used to attenuate the mismatched disturbances [13]. In addition, a mixed H_2/H_∞ robust controller is introduced for the tracking control of a generic hypersonic vehicle [14]. To enhance the robustness, the T-S fuzzy model is employed to estimate the lumped uncertainty, and the disturbance observer is used to estimate the external disturbances. Moreover, a finite-time H_∞ control is used for the design of the fault-tolerant controller for the reentry vehicles, resulting in a good robustness for the control delay, input constraints, and parameter perturbation [15]. Secondly, μ-Synthesis theory has been widely applied in engineering as a robust approach. A μ-synthesis controller is designed for the supercavitating vehicle to achieve the bank-to-turn (BTT) control, and the stability of the tunning process is guaranteed [16]. To ensure the robustness over the entire working envelope of the flight environment testbed, a μ-synthesis controller based on LPV system is firstly designed [17]. Thirdly, the robust adaptive control has attracted strong interest from researchers because of its excellent robust performance. Based on the model-reference adaptive control (MRAC), a modified adaptive law is designed to avoid the parameters drift and the wind-up effect of integrators [18]. To obtain guaranteed transient performance, a modified MRAC named the L_1 adaptive control is applied to the linear infinite-dimensional systems [19] and the multi-input multi-output (MIMO) systems [20]. Noting that the conventional MRAC faces the difficulties in choosing the Lyapunov function, the immersion and invariance (I&I) adaptive control is proposed [21]. The I&I method makes the design of adaptive law more flexible because there is no need to construct the Lyapunov function. Liu *et al*. adopted the I&I method to design the observers for the unmeasurable states of AHV, and the strong robustness against the uncertainties is demonstrated by comparison simulation [22]. Furthermore, the intelligent algorithms, such as neural network and fuzzy logic system (FLS), have been combined with the adaptive control. A neuro-adaptive controller is designed for the output tracking of AHV, and a reinforcement learning mechanism is particularly constructed for the weights updating of neural network [23]. Based on the interval T2-FLSs, the unknown dynamics of AHV is approximated, and the robustness is guaranteed under the influence of the parameter perturbation, unmeasurable states, and measurement noises [24].

Motivated by the above literatures, a robust controller with an adaptive projection-based parameter estimator is presented for AHV. The control-oriented model is firstly studied. The parameter-varying model can well characterize the model uncertainty, especially parameter perturbation [25]. Moreover, other characteristics, such as the structural elasticity and aero-propulsive coupling, can also be described in the parameter-varying model. In the previous study, the number of variable parameters selected in the parameter-varying model was relatively large, resulting in the problem of over-parameterization and the increased complexity of controller design procedure [26], [27]. To avoid the mentioned problem, a novel parameter-varying model is established wherein the number of variable parameters is significantly reduced. Then, the framework of controller is established by adopting the backstepping approach, in which a second-order filter is introduced to solve the problem of ''explosion of terms''. In order to enhance the robustness of the controller, an adaptive parameter estimator is introduced. Noting that the parameter estimation is achieved by a chain of integrators in engineering, the saturation of integrator should be considered in the process of designing the adaptive law. Thus, a sufficiently smooth projection operator [28] is introduced to guarantee the uniform boundedness of adaptive parameters. Also, the Lipschitz continuous dead-zone modification is used to avoid the problem of parameter draft in the conventional adaptive control. The main contributions of this paper are listed as follows:

i) A novel parameter-varying model is established wherein the number of variable parameters is significantly reduced, avoiding the problem of overparameterization and simplifying the procedure of controller design.

ii) An adaptive law combining the Lipschitz continuous dead-zone modification and the sufficiently smooth projection operator is designed, resulting in the uniform boundedness of variable parameters.

The outline of this article is as follows. In Section 2, the description of the AHV model is given, and the framework of the controller is described. Section 3 gives the design of the nominal controller and the robust controller with adaptive projection-based parameter estimation in detail. Numerical simulations of two controllers are given in Section 4 and Section 5 gives the conclusion.

II. MODELING DESCRIPTION AND CONTROLLER FRAMEWORK

A. MODEL DESCRIPTION

The model established by Parker *et al.* can describe the main dynamic characteristics of AHV and is widely used in the design of flight control system [29]. The kinematics and dynamics equations of AHV are given as follows:

$$\dot{V} = \frac{1}{m}\left[T\cos(\theta-\gamma) - D\right] - g\sin\gamma, \tag{1}$$

$$\dot{h} = V\sin\gamma, \tag{2}$$

$$\dot{\gamma} = \frac{1}{mV}\left[L + T\sin(\theta-\gamma)\right] - \frac{g}{V}\cos\gamma, \tag{3}$$

$$\dot{\theta} = Q, \tag{4}$$

$$I_{yy}\dot{Q} = M + \tilde{\psi}_1\ddot{\eta}_1 + \tilde{\psi}_2\ddot{\eta}_2, \tag{5}$$

$$k_1\ddot{\eta}_1 = -2\zeta_1\omega_1\dot{\eta}_1 - \omega_1^2\eta_1 + N_1 - \tilde{\psi}_1\frac{M}{I_{yy}} - \frac{\tilde{\psi}_1\tilde{\psi}_2\ddot{\eta}_2}{I_{yy}}, \tag{6}$$

$$k_2\ddot{\eta}_2 = -2\zeta_2\omega_2\dot{\eta}_2 - \omega_2^2\eta_2 + N_2 - \tilde{\psi}_2\frac{M}{I_{yy}} - \frac{\tilde{\psi}_2\tilde{\psi}_1\ddot{\eta}_1}{I_{yy}}, \tag{7}$$

where the rigid states $\boldsymbol{x} = [V, h, \gamma, \theta, Q]$ are the velocity, altitude, flight path angle(FPA), pitch angle and pitch rate, respectively. $\boldsymbol{\eta} = [\eta_1, \dot{\eta}_1, \eta_2, \dot{\eta}_2]$ denotes the flexible states. The thrust T, lift L, drag D, pitching moment M and generalized elastic forces $N_i (i = 1, 2)$ are shown as follows [29]:

$$\begin{cases} L \approx \bar{q}S(C_L^{\alpha}\alpha + C_T^{\delta_e}\delta_e + C_L^0) \\ D \approx \bar{q}S(CD^{\alpha^2}\alpha^2 + C_D^{\alpha}\alpha + C_D^{\delta_e^2}\delta_e^2 + C_D^{\delta_e}\delta_e + C_D^0) \\ T \approx C_T^{\alpha^3}\alpha^3 + C_T^{\alpha^2}\alpha^2 + C_T^{\alpha}\alpha + C_T^0 \\ M \approx z_T T + \bar{q}S\bar{c}(C_{M,\alpha}^{\alpha^2}\alpha^2 + C_{M,\alpha}^{\alpha}\alpha + C_{M,\alpha}^0 + c_e\delta_e) \\ N_i = N_i^{\alpha^2}\alpha^2 + N_i^{\alpha}\alpha + N_i^{\delta_e}\delta_e + N_i^0, i = 1, 2 \end{cases} \tag{8}$$

with

$$\begin{aligned} C_T^{\alpha^3} &= \beta_1(h, \bar{q})\,\Phi + \beta_2(h, \bar{q}), \\ C_T^{\alpha^2} &= \beta_3(h, \bar{q})\,\Phi + \beta_4(h, \bar{q}), \\ C_T^{\alpha} &= \beta_5(h, \bar{q})\,\Phi + \beta_6(h, \bar{q}), \\ C_T^0 &= \beta_7(h, \bar{q})\,\Phi + \beta_8(h, \bar{q}), \\ \bar{q} &= \frac{1}{2}\bar{\rho}V^2, \bar{\rho} = \bar{\rho}_0\exp\left(-\frac{h-h_0}{h_s}\right), \end{aligned}$$

where Φ denotes the fuel equivalence ratio, and δ_e is the elevator deflection; α is the angle of attack (AOA); $\bar{q}$ is the dynamic pressure, and $\bar{\rho}$ is the air density.

The model parameters are derived from [30], and the coefficients of aerodynamic forces and thrust are given by [29]. The value of the above parameters are given in the Appendix as Table 2-6.

B. CONTROLLER FRAMEWORK

Inspired by the work of Fiorentini *et al.*, the AHV model is decomposed into the V − *subsystem* and the h − *subsystem* [31]. The control target is to adjust the value of the control inputs $u = [\Phi, \delta_e]^{\mathrm{T}}$ so that the outputs $y = [V, h]^{\mathrm{T}}$ can follow their reference commands $y_{\mathrm{ref}} = [V_{\mathrm{ref}}, h_{\mathrm{ref}}]^{\mathrm{T}}$. V − *subsystem* is a first-order dynamic system described as Eq. (1), and h − *subsystem* consists of a four-order dynamic system described as Eqs. (2)∼(5). In order to reduce the order of the h − *subsystem* and simplify the controller design procedure, a command transform from the reference commands h_d to the FPA command γ_d is designed as [32]:

$$\gamma_d = \arcsin\left(\frac{-k\tilde{h} - k_I\int_0^t \tilde{h}d\tau + \dot{h}_{\mathrm{ref}}}{V}\right), \tag{9}$$

where $k > 0, k_I > 0$ are the proportional and integral (PI) coefficients, respectively; $\tilde{h} = h - h_{\mathrm{ref}}$ is the tracking error.

According to [32], $\tilde{h}$ can converge to zero exponentially, if $\gamma \to \gamma_d$ is satisfied. Assume that the rigid states $\boldsymbol{x} = [V, h, \gamma, \theta, Q]$ are all measurable. Although the small FPA and AOA are not easy to measure, the advanced sensor system and state reconstruction algorithm can provide the measurement of the states that satisfies the accuracy requirement. Thus, the assumption that the rigid states are completely measurable is reasonable. Since the flexible states $\boldsymbol{\eta}$ are unmeasurable and the mechanism for actively suppressing the structural elasticity is lacking, the feedback of $\boldsymbol{\eta}$ is not taken into account during the controller design. The influence of the structural elasticity is weakened by enhancing the robustness of the controller. It should be noted that the model adopted in this paper [29] includes the canard δ_c, whose main function is to adaptively compensate for the lift loss caused by the deflection of the elevator and avoid the non-minimum phase behavior. In order to avoid the problem of "explosion of terms" in the conventional backstepping, the second-order filter presented by Polycarpou *et al.* is introduced [33]. The framework of controller is summarized as Fig.1.

III. CONTROLLER DESIGN AND STABILITY ANALYSIS

In this section, a robust controller with adaptive projection-based parameter estimation is introduced for the AHV model described as Eqs. (1)∼(7). Noting that the design of nominal controller is the basis for model analysis and controller design, a nominal controller is firstly designed. Then, a parameter-varying model with fewer parameters is established. Based on the proposed parameter-varying model, an adaptive robust controller is designed by combining the Lipschitz continuous dead-zone modification and the sufficiently smooth projection operator. Furthermore, the stability analysis for the designed controller is carried out based on Lyapunov theory.

A. NOMINAL CONTROLLER DESIGN

Before designing the controller, the model is firstly transformed into a strict feedback form. The V − *subsystem* is rewritten as

$$\dot{V} = f_V + g_V\Phi \tag{10}$$

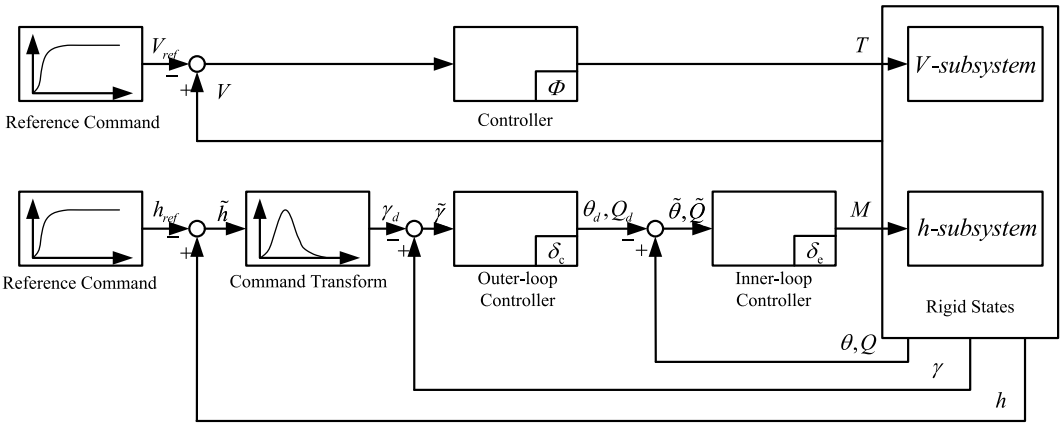

FIGURE 1. Framework of the controller.

with

$$f_V = \frac{\cos\alpha}{m}\left[\beta_2\alpha^3 + \beta_4\alpha^2 + \beta_6\alpha + \beta_8\right] - \frac{\bar{q}S}{m}\left(C_D^{\alpha^2}\alpha^2 + C_D^{\alpha}\alpha + C_D^0\right) - g\sin\gamma$$
$$g_V = \frac{\cos\alpha}{m}\left[\beta_1\alpha^3 + \beta_3\alpha^2 + \beta_5\alpha + \beta_7\right] \neq 0.$$

Similarly, the dynamic equations of $h-subsystem$ are described as

$$\begin{cases}\dot{\gamma} = f_\gamma + g_\gamma\theta \\ \dot{\theta} = Q \\ \dot{Q} = f_Q + g_Q\delta_e\end{cases} \tag{11}$$

with

$$f_\gamma = \frac{\bar{q}S\left(C_L^0 - C_L^\alpha\gamma\right) + T\sin\alpha}{mV} - g\cos\gamma, \quad g_\gamma = \frac{\bar{q}SC_L^\alpha}{mV} \neq 0,$$
$$f_Q = \frac{z_T T + \bar{q}S\bar{c}C_{M,\alpha}(\alpha)}{I_{yy}}, \quad g_Q = \frac{\bar{q}S\bar{c}c_e}{I_{yy}} \neq 0.$$

Then, a nominal controller is designed. Define the velocity tracking error as $\tilde{V} = V - V_{\text{ref}}$. Differentiating $\tilde{V}$ by time t, we have

$$\dot{\tilde{V}} = g_V\Phi + f_V - \dot{V}_{\text{ref}}. \tag{12}$$

The control law Φ is designed as

$$\Phi = g_V^{-1}\left(-k_{V1}\tilde{V} - k_{V2}\int_0^t \tilde{V}\mathrm{d}\tau - f_V + \dot{V}_{\text{ref}}\right), \tag{13}$$

where $k_{V1} > 0, k_{V2} > 0$ are the PI coefficients.

For the $h-subsystem$, the procedure of designing the controller, based on the proposed controller framework, is divided into the following three steps.

Step 1: Define the PFA tracking error as $\tilde{\gamma} = \gamma - \gamma_{\text{d}}$. Differentiating $\tilde{\gamma}$ by time t, we have

$$\dot{\tilde{\gamma}} = g_\gamma\theta + f_\gamma - \dot{\gamma}_{\text{d}}. \tag{14}$$

The virtual control law θ_c is designed as

$$\theta_c = g_\gamma^{-1}\left(-k_{\gamma1}\tilde{\gamma} - k_{\gamma2}\int_0^t \tilde{\gamma}\mathrm{d}\tau - f_\gamma + \dot{\gamma}_{\text{d}}\right), \tag{15}$$

where $k_{\gamma1} > 0, k_{\gamma2} > 0$ are the PI coefficients.

Step 2: Let θ_{d} and $\dot{\theta}_{\text{d}}$ be the tracking and differential signals obtained by introducing the second-order filter [33] to process the virtual control law θ_c. Define the tracking error of the pitch angle as $\tilde{\theta} = \theta - \theta_{\text{d}}$. Differentiating $\tilde{\theta}$ by time t, we have

$$\dot{\tilde{\theta}} = Q - \dot{\theta}_{\text{d}}. \tag{16}$$

The virtual control law Q_c is designed as

$$Q_c = -k_{\theta1}\tilde{\theta} - k_{\theta2}\int_0^t \tilde{\theta}\mathrm{d}\tau - g_\gamma\tilde{\gamma} + \dot{\theta}_{\text{d}}, \tag{17}$$

where $k_{\theta1} > 0, k_{\theta2} > 0$ are the PI coefficients.

Step 3: Let Q_{d} and $\dot{Q}_{\text{d}}$ be the tracking and differential signals obtained by introducing the second-order filter [33] to process the virtual control law Q_c. Define the tracking error of the pitch rate as $\tilde{Q} = Q - Q_{\text{d}}$. Differentiating $\tilde{Q}$ by time t, we have

$$\dot{\tilde{Q}} = g_Q\delta_e + f_Q - \dot{Q}_{\text{d}}. \tag{18}$$

The control law δ_e is designed as

$$\delta_e = g_Q^{-1}\left(-k_{Q1}\tilde{Q} - k_{Q2}\int_0^t \tilde{Q}\mathrm{d}\tau - f_Q - \tilde{\theta} + \dot{Q}_{\text{d}}\right) \tag{19}$$

where $k_{Q1} > 0, k_{Q2} > 0$ are the PI coefficients.

Next, we prove the stability of the close-loop system consisting of the designed nominal controller and AHV model using the Lyapunov theory.

For the $V-subsystem$, the Lyapunov function is selected as follows:

$$W_V = \frac{\tilde{V}^2}{2} + \frac{k_{V2}}{2}\left(\int_0^t \tilde{V}\mathrm{d}\tau\right)^2. \tag{20}$$

Differentiating W_V by time t and invoking (12) and (13) yields

$$\begin{aligned}\dot{W}_V &= \tilde{V}\dot{\tilde{V}} + k_{V2}\tilde{V}\int_0^t \tilde{V}\mathrm{d}\tau \\ &= \tilde{V}\left(f_V + g_V\left[g_V^{-1}\left(-k_{V1}\tilde{V} - k_{V2}\int_0^t \tilde{V}\mathrm{d}\tau - f_V + \dot{V}_{\text{ref}}\right)\right] - \dot{V}_{\text{ref}}\right) + k_{V2}\tilde{V}\int_0^t \tilde{V}\mathrm{d}\tau \\ &= -k_{V1}\tilde{V}^2\end{aligned} \tag{21}$$

Define the tracking errors of the second-order filter [33] as $y_1 = \theta_d - \theta_c$ and $y_2 = Q_d - Q_c$. By selecting the appropriate natural frequency and damping ratio, there exist the positive constants $\bar{y}_1$, $\bar{y}_2$, such that $|y_1| \le \bar{y}_1$, and $|y_2| \le \bar{y}_2$ hold. For the $h-$ *subsystem*, the Lyapunov function is selected as follows

$$W_h = \frac{\tilde{\gamma}^2}{2} + \frac{k_{\gamma 2}}{2}\left(\int_0^t \tilde{\gamma}\mathrm{d}\tau\right)^2 + \frac{\tilde{\theta}^2}{2} + \frac{k_{\theta 2}}{2}\left(\int_0^t \tilde{\theta}\mathrm{d}\tau\right)^2 + \frac{\tilde{Q}^2}{2} + \frac{k_{Q2}}{2}\left(\int_0^t \tilde{Q}\mathrm{d}\tau\right)^2 \quad (22)$$

Taking time derivative along (22), we have

$$\dot{W}_h = \tilde{\gamma}\dot{\tilde{\gamma}} + k_{\gamma 2}\tilde{\gamma}\int_0^t \tilde{\gamma}\mathrm{d}\tau + \tilde{\theta}\dot{\tilde{\theta}} + k_{\theta 2}\tilde{\theta}\int_0^t \tilde{\theta}\mathrm{d}\tau + \tilde{Q}\dot{\tilde{Q}} + k_{Q2}\tilde{Q}\int_0^t \tilde{Q}\mathrm{d}\tau \quad (23)$$

Substituting (15) into (14) yields

$$\begin{aligned}\dot{\tilde{\gamma}} &= f_\gamma + g_\gamma(\theta - \theta_d + \theta_d - \theta_c + \theta_c) - \dot{\gamma}_d \\ &= f_\gamma + g_\gamma\left(\tilde{\theta} + y_1 + \theta_c\right) - \dot{\gamma}_d \\ &= f_\gamma + g_\gamma\left(\tilde{\theta} + y_1 + \left[g_\gamma^{-1}\left(-k_{\gamma 1}\tilde{\gamma} - k_{\gamma 2}\int_0^t \tilde{\gamma}\mathrm{d}\tau - f_\gamma + \dot{\gamma}_d\right)\right]\right) - \dot{\gamma}_d \\ &= -k_{\gamma 1}\tilde{\gamma} - k_{\gamma 2}\int_0^t \tilde{\gamma}\mathrm{d}\tau + g_\gamma\tilde{\theta} + g_\gamma y_1 \end{aligned} \quad (24)$$

Similarly, we have

$$\dot{\tilde{\theta}} = -k_{\theta 1}\tilde{\theta} - k_{\theta 2}\int_0^t \tilde{\theta}\mathrm{d}\tau - g_\gamma\tilde{\gamma} + \tilde{Q} + y_2 \quad (25)$$

$$\dot{\tilde{Q}} = -k_{Q1}\tilde{Q} - k_{Q2}\int_0^t \tilde{Q}\mathrm{d}\tau - \tilde{\theta} \quad (26)$$

Substituting (24)$\sim$ (26) into (23) yields

$$\dot{W}_h = -k_{\gamma 1}\tilde{\gamma}^2 - k_{\theta 1}\tilde{\theta}^2 - k_{Q1}\tilde{Q}^2 + g_\gamma y_1\tilde{\gamma} + y_2\tilde{\theta} \quad (27)$$

Since

$$g_\gamma y_1\tilde{\gamma} \le |g_\gamma|\,|y_1\tilde{\gamma}| \le |g_\gamma|\left(\frac{\bar{y}_1^2}{2} + \frac{\tilde{\gamma}^2}{2}\right), \quad y_2\tilde{\theta} \le \frac{\bar{y}_2^2}{2} + \frac{\tilde{\theta}^2}{2},$$

the Eq. (27) satisfies the following inequalities

$$\dot{W}_h \le -\left(k_{\gamma 1} - \frac{|g_\gamma|}{2}\right)\tilde{\gamma}^2 - \left(k_{\theta 1} - \frac{1}{2}\right)\tilde{\theta}^2 - k_{Q1}\tilde{Q}^2 + \frac{|g_\gamma|\bar{y}_1^2}{2} + \frac{\bar{y}_2^2}{2} \quad (28)$$

Choosing $k_{\gamma 1} > |g_\gamma|/2$ and $k_{\theta 1} > 1/2$, the compact sets are defined as

$$\begin{cases} \Omega_{\tilde{\gamma}} = \left\{\tilde{\gamma}\,\middle|\,|\tilde{\gamma}| \le \sqrt{\left(\frac{|g_\gamma|\bar{y}_1^2}{2} + \frac{\bar{y}_2^2}{2}\right)\Big/\left(k_{\gamma 1} - \frac{|g_\gamma|}{2}\right)}\right\} \\ \Omega_{\tilde{\theta}} = \left\{\tilde{\theta}\,\middle|\,|\tilde{\theta}| \le \sqrt{\left(\frac{|g_\gamma|\bar{y}_1^2}{2} + \frac{\bar{y}_2^2}{2}\right)\Big/\left(k_{\theta 1} - \frac{1}{2}\right)}\right\} \\ \Omega_{\tilde{Q}} = \left\{\tilde{Q}\,\middle|\,|\tilde{Q}| \le \sqrt{\left(\frac{|g_\gamma|\bar{y}_1^2}{2} + \frac{\bar{y}_2^2}{2}\right)\Big/k_{Q1}}\right\} \end{cases} \quad (29)$$

The radiuses of compact sets described as Eq. (29) can be arbitrarily small by selecting enough large $k_{\gamma 1}$, $k_{\theta 1}$ and k_{Q1}. The inequalities $\dot{W}_V < 0$ holds for $\tilde{V} \ne 0$, and $\dot{W}_h < 0$ holds when the tracking error is not within compact sets described as Eq. (29). According to the Lyapunov theory, the tracking error $\tilde{V}$ and $\tilde{\gamma}$ are bounded. Therefore, the proposed nominal controller can make $V \to V_{\mathrm{ref}}$ and $\gamma \to \gamma_d$. Furthermore, we obtain $h \to h_{\mathrm{ref}}$ [32].

B. ROBUST CONTOLLER WITH ADAPTIVE PROJECTION-BASED PARAMETER ESTIMATION

1) THE PARAMETER-VARYING MODEL

The variable parameters of the model are mainly composed of the aerodynamic coefficients and thrust coefficients. The parameter-varying model is derived from the model with a strict feedback form [25]. In order to describe the idea of building the parameter-varying model in detail, the $V-$ *subsystem* is taken as an example. In [25]–[27], the variable parameters in f_V and g_V are fully described in a separate way. Since f_V and g_V contain the same items, the above approach will lead to the problem of overparameterization. Moreover, the complexity of controller design will be increased. Thus, It is necessary to further optimize the parameter-varying model. A novel parameter-varying model is established in this paper. The main idea is to reduce the number of variable parameters by merging the parameters with same items. The establishment of the parameter-varying model is given as follows.

Assume that the parameter perturbation caused by model uncertainty has the following form [34]:

$$\begin{cases} \Delta\Theta(\boldsymbol{x}, t) = \sigma(t)\cdot\overline{\Theta}(\boldsymbol{x}) \\ \sigma(t) = Ae^{\kappa t}\sin(\omega t) \end{cases} \quad (30)$$

where $\sigma(t)$ is the deviation function that reflects the relationship between the perturbation value and the nominal value of the parameter; $A > 0$, $\kappa < 0$ and $\omega > 0$ denote the maximum amplitude of the perturbation, the decay rate and the frequency, respectively.

Substituting (8) into (1), (3), (5) and taking the parameter perturbation into account, we obtain the following Eqs. (31)$\sim$(33). (described in the bottom of the next page)

For the $V-$ *subsystem*, the varying-parameter form obtained by the method in [26], [27] is given below for comparison. Let $C_{T\Phi}^{\alpha^3} = \beta_1/\bar{q}S$, $C_{T\Phi}^{\alpha^2} = \beta_3/\bar{q}S$, $C_{T\Phi}^{\alpha} = \beta_5/\bar{q}S$,

$C_{T\Phi}^{0} = \beta_7/\bar{q}S$, $C_{T0}^{\alpha^3} = \beta_2/\bar{q}S$, $C_{T0}^{\alpha^2} = \beta_4/\bar{q}S$, $C_{T0}^{\alpha} = \beta_6/\bar{q}S$, $C_{T0}^{0} = \beta_8/\bar{q}S$, the Eq. (31) is rewritten as

$$\dot{V} = \left(\bar{\boldsymbol{\omega}}_{gv}^{\mathrm{T}}\bar{\boldsymbol{\theta}}_{gv}\right)\Phi + \bar{\boldsymbol{\omega}}_{fv}^{\mathrm{T}}\bar{\boldsymbol{\theta}}_{fv} - g\sin\gamma \tag{34}$$

where

$$\bar{\boldsymbol{\omega}}_{fv} = \bar{q}S\left[\alpha^3\cos\alpha\ \alpha^2\cos\alpha\ \alpha\cos\alpha\ \cos\alpha - \alpha^2 - \alpha - 1\right]^{\mathrm{T}}$$
$$\bar{\boldsymbol{\theta}}_{fv} = \frac{(1+\Delta)}{m}\left[C_{T0}^{\alpha^3}\ C_{T0}^{\alpha^2}\ C_{T0}^{\alpha}\ C_{T0}^{0}\ C_{D}^{\alpha^2}\ C_{D}^{\alpha}\ C_{D}^{0}\right]^{\mathrm{T}}$$
$$\bar{\boldsymbol{\omega}}_{gv} = \bar{q}S\left[\alpha^3\cos\alpha\ \alpha^2\cos\alpha\ \alpha\cos\alpha\ \cos\alpha\right]^{\mathrm{T}}$$
$$\bar{\boldsymbol{\theta}}_{gv} = \frac{(1+\Delta)}{m}\left[C_{T\Phi}^{\alpha^3}\ C_{T\Phi}^{\alpha^2}\ C_{T\Phi}^{\alpha}\ C_{T\Phi}^{0}\right]^{\mathrm{T}}$$

It can be seen from Eq. (34) that the items in $\bar{\boldsymbol{\omega}}_{gv}$ are all included in $\bar{\boldsymbol{\omega}}_{fv}$. Thus, in order to simplify the parameter-varying model, g_V is selected as the same as the Eq. (10), that is, g_V is only related to the nominal value. The error between the actual value and the nominal value of g_V can be reflected in the time-varying parameters of f_V. Through the above approach, the controller design can be greatly simplified, and the problem of overparameterization can be avoided. Based on the above analysis, different from the Eq. (34), we have

$$\dot{V} = g_V\Phi + \boldsymbol{\omega}_{fv}^{\mathrm{T}}\boldsymbol{\theta}_{fv} - g\sin\gamma, \tag{35}$$

where $\boldsymbol{\omega}_{fv}$, $\boldsymbol{\theta}_{fv}$, as shown at the bottom of this page.

Similarly, for the $h-$ *subsystem*, the Eq. (32) is rewritten as

$$\dot{\gamma} = g_\gamma\theta + \boldsymbol{\omega}_{f\gamma}^{\mathrm{T}}\boldsymbol{\theta}_{f\gamma} - \frac{g}{V}\cos\gamma, \tag{36}$$

where $\boldsymbol{\omega}_{f\gamma}$, $\boldsymbol{\theta}_{f\gamma}$, as shown at the bottom of this page.

Let d_η be the influence on the variable parameters caused by the flexible states. Similarly, the Eq. (33) is rewritten as

$$\dot{Q} = g_Q\delta_{\mathrm{e}} + \boldsymbol{\omega}_{fQ}^{\mathrm{T}}\boldsymbol{\theta}_{fQ}, \tag{37}$$

where $\boldsymbol{\omega}_{fQ}$, $\boldsymbol{\theta}_{fQ}$, as shown at the bottom of this page.

$$\dot{V} = (1+\Delta)\cdot\left[\frac{\begin{array}{l}\Phi\cdot\left(\beta_1\alpha^3+\beta_3\alpha^2+\beta_5\alpha+\beta_7\right)\cos\alpha+\left(\beta_2\alpha^3+\beta_4\alpha^2+\beta_6\alpha+\beta_8\right)\cos\alpha\\ -\bar{q}S\left(C_D^{\alpha^2}\alpha^2+C_D^{\alpha}\alpha+C_D^{0}\right)\end{array}}{m}\right] - g\sin\gamma \tag{31}$$

$$\dot{\gamma} = (1+\Delta)\cdot\left[\frac{\bar{q}SC_L^{\alpha}}{mV}\theta + \frac{\begin{array}{l}\bar{q}S\left(-C_L^{\alpha}\gamma+C_L^{0}\right)+\left(\beta_1\alpha^3+\beta_3\alpha^2+\beta_5\alpha+\beta_7\right)\Phi\sin\alpha\\ +\left(\beta_2\alpha^3+\beta_4\alpha^2+\beta_6\alpha+\beta_8\right)\sin\alpha\end{array}}{mV}\right] - \frac{g}{V}\cos\gamma \tag{32}$$

$$\begin{aligned}\dot{Q} = \frac{(1+\Delta)}{I_{\mathrm{yy}}}\cdot\Big[&z_T\left(\left(\beta_1\alpha^3+\beta_3\alpha^2+\beta_5\alpha+\beta_7\right)\Phi+\left(\beta_2\alpha^3+\beta_4\alpha^2+\beta_6\alpha+\beta_8\right)\right)\\ &+\bar{q}S\bar{c}\left(C_{M,\alpha}^{\alpha^2}\alpha^2+C_{M,\alpha}^{\alpha}\alpha+C_{M,\alpha}^{0}+c_{\mathrm{e}}\delta_{\mathrm{e}}\right)+d_\eta\Big]\end{aligned} \tag{33}$$

$$\boldsymbol{\omega}_{fv} = \bar{q}S\left[\alpha^3\cos\alpha\quad\alpha^2\cos\alpha\quad\alpha\cos\alpha\quad\cos\alpha-\alpha^2-\alpha-1\right]^{\mathrm{T}}$$
$$\boldsymbol{\theta}_{fv} = \frac{1}{m}\begin{bmatrix}C_{T0}^{\alpha^3}+\Delta & (C_{T0}^{\alpha^3}+C_{T\Phi}^{\alpha^3}\Phi) & C_{T0}^{\alpha^2}+\Delta & (C_{T0}^{\alpha^2}+C_{T\Phi}^{\alpha^2}\Phi)\\ C_{T0}^{\alpha}+\Delta & (C_{T0}^{\alpha}+C_{T\Phi}^{\alpha}\Phi) & C_{T0}^{0}+\Delta(C_{T0}^{0}+C_{T\Phi}^{0}\Phi) & \\ (1+\Delta)C_D^{\alpha^2} & (1+\Delta)C_D^{\alpha} & (1+\Delta)C_D^{0} & \end{bmatrix}^{\mathrm{T}}.$$

$$\boldsymbol{\omega}_{f\gamma} = \frac{\bar{q}S}{V}\begin{bmatrix}\alpha^3\Phi\sin\alpha & \alpha^2\Phi\sin\alpha & \alpha\Phi\sin\alpha\Phi\sin\alpha\\ \alpha^3\sin\alpha & \alpha^2\sin\alpha & \alpha\sin\alpha & \sin\alpha-\gamma 1\end{bmatrix}^{\mathrm{T}},$$
$$\boldsymbol{\theta}_{f\gamma} = \frac{1}{m}\begin{bmatrix}(1+\Delta)C_{T\Phi}^{\alpha^3} & (1+\Delta)C_{T\Phi}^{\alpha^2}(1+\Delta)C_{T\Phi}^{\alpha} & (1+\Delta)C_{T\Phi}^{0}\\ (1+\Delta)C_{T0}^{\alpha^3} & (1+\Delta)C_{T0}^{\alpha^2}(1+\Delta)C_{T0}^{\alpha} & (1+\Delta)C_{T0}^{0}\\ (1+\Delta)C_L^{\alpha} & (1+\Delta)C_L^{0}+\Delta C_L^{\alpha}\theta & \end{bmatrix}^{\mathrm{T}}.$$

$$\boldsymbol{\omega}_{fQ} = \bar{q}S\left[\alpha^3\Phi\quad\alpha^2\Phi\quad\alpha\Phi\quad\Phi\alpha^3\alpha^2\alpha 1\right]^{\mathrm{T}},$$
$$\boldsymbol{\theta}_{fQ} = \frac{1+\Delta}{I_{\mathrm{yy}}}\begin{bmatrix}z_TC_{T\Phi}^{\alpha^3} & z_TC_{T\Phi}^{\alpha^2}z_TC_{T\Phi}^{\alpha} & z_TC_{T\Phi}^{0}\\ z_TC_{T0}^{\alpha^3} & \left(z_TC_{T0}^{\alpha^2}+\bar{c}C_{M,\alpha}^{\alpha^2}\right) & \left(z_TC_{T0}^{\alpha}+\bar{c}C_{M,\alpha}^{\alpha}\right)\\ \left(z_TC_{T0}^{0}+\bar{c}C_{M,\alpha}^{0}+\bar{c}\Delta c_{\mathrm{e}}\delta_{\mathrm{e}}+d_\eta\right) & & \end{bmatrix}^{\mathrm{T}}.$$

In summary, the $h-$ *subsystem* is converted into a strict feedback system with a parameter-varying form as follows:

$$\begin{cases} \dot{\gamma} = g_\gamma \theta + \boldsymbol{\omega}_{f\gamma}^{\mathrm{T}} \boldsymbol{\theta}_{f\gamma} - \dfrac{g}{V}\cos\gamma \\ \dot{\theta} = Q \\ \dot{Q} = g_Q \delta_{\mathrm{e}} + \boldsymbol{\omega}_{fQ}^{\mathrm{T}} \boldsymbol{\theta}_{fQ} \end{cases} \tag{38}$$

2) CONTROLLER DESIGN

For the $V-$ *subsystem*, differentiating $\tilde{V}$ by time t, we have

$$\dot{\tilde{V}} = g_V \Phi + \boldsymbol{\omega}_{fv}^{\mathrm{T}} \boldsymbol{\theta}_{fv} - g\sin\gamma - \dot{V}_{\mathrm{ref}}. \tag{39}$$

According to the idea of controller design in the Section III.A, the control law is Φ designed as

$$\Phi = g_V^{-1}\left(-k_{V1}\tilde{V} - k_{V2}\int_0^t \tilde{V}\mathrm{d}\tau - \boldsymbol{\omega}_{fv}^{\mathrm{T}}\hat{\boldsymbol{\theta}}_{fv} + g\sin\gamma + \dot{V}_{\mathrm{ref}}\right), \tag{40}$$

where $\hat{\dot{\boldsymbol{\theta}}}_{fv}$ is the estimated value of $\boldsymbol{\theta}_{fv}$.

The adaptive law of $\hat{\dot{\boldsymbol{\theta}}}_{fv}$ is designed as

$$\hat{\dot{\boldsymbol{\theta}}}_{fv} = \Gamma_{fv}\boldsymbol{\omega}_{fv}\tilde{V}, \tag{41}$$

where the diagonal matrix Γ_{fv} is the designed parameter.

To avoid the parameter draft, the adaptive law shown in the Eq. (41) is modified with the dead-zone modification in this paper. Since the function of dead-zone modification is not Lipschitz continuous, high-frequency oscillation will occur when the tracking error approaches the preset boundary. To avoid the high-frequency oscillation, a modified function of dead-zone modification which is Lipschitz continuous is introduced as follows [18]:

$$\mu(\|e\|, e_0, b) = \max(0, \min(1, \frac{\|e\| - be_0}{(1-b)e_0})), \tag{42}$$

where e_0 and $0 < b < 1$ are the designed parameters.

The schematic diagram of the function described as the Eq. (42) is shown in Fig. 2.

The modified adaptive law is designed as

$$\hat{\dot{\boldsymbol{\theta}}}_{fv} = \Gamma_{fv}\boldsymbol{\omega}_{fv}\tilde{V}\mu(\left|\tilde{V}\right|, \tilde{V}_0, b_V), \tag{43}$$

where $\tilde{V}_0 > 0$ and $0 < b_V < 1$ are the designed parameters.

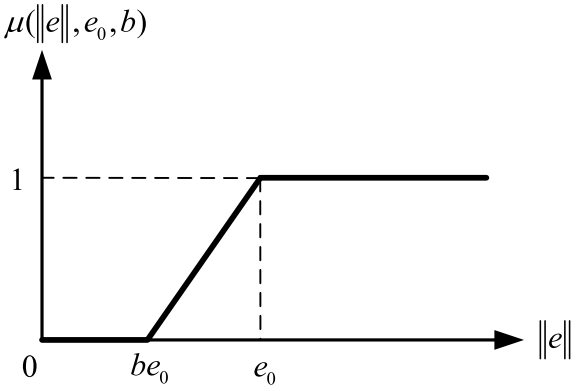

FIGURE 2. Schematic diagram of $\mu(\|e\|, e_0, b)$.

To guarantee the boundedness of adaptive parameters, a sufficiently smooth projection operator is introduced [28]. The adaptive law is redesigned as

$$\hat{\dot{\boldsymbol{\theta}}}_{fv} = \mathrm{Proj}(\hat{\boldsymbol{\theta}}_{fv}, \Gamma_{fv}\boldsymbol{\omega}_{fv}\tilde{V}\mu(\left|\tilde{V}\right|, \tilde{V}_0, b_V)). \tag{44}$$

According to the definition of the projection operator [28], the Eq. (44) is rewritten as (45), as shown at the bottom of this page, where ε_V, δ_V, and $\theta_{fv}^{\max}$ are the designed parameters.

For the $h-$ *subsystem*, the procedure of designing the controller is divided into the following three steps.

Step 1: Differentiating $\tilde{\gamma}$ by time t, we obtain

$$\dot{\tilde{\gamma}} = g_\gamma\theta + \boldsymbol{\omega}_{f\gamma}^{\mathrm{T}}\boldsymbol{\theta}_{f\gamma} - \frac{g}{V}\cos\gamma - \dot{\gamma}_{\mathrm{d}}. \tag{46}$$

The virtual control law θ_c is designed as

$$\theta_c = g_\gamma^{-1}\left(-k_{\gamma1}\tilde{\gamma} - k_{\gamma2}\int_0^t \tilde{\gamma}\mathrm{d}\tau - \boldsymbol{\omega}_{f\gamma}^{\mathrm{T}}\hat{\boldsymbol{\theta}}_{f\gamma} + \frac{g}{V}\cos\gamma + \dot{\gamma}_{\mathrm{d}}\right), \tag{47}$$

where $\hat{\boldsymbol{\theta}}_{f\gamma}$ is the estimated value of $\boldsymbol{\theta}_{f\gamma}$.

Similar to the $V-$ *subsystem*, the adaptive law based on the Lipschitz continuous dead-zone modification and the sufficiently smooth projection operators is designed as

$$\hat{\dot{\theta}}_{f\gamma} = \mathrm{Proj}\left(\hat{\boldsymbol{\theta}}_{f\gamma}, \Gamma_{f\gamma}\boldsymbol{\omega}_{f\gamma}\tilde{\gamma}\mu\left(\tilde{\gamma}|\tilde{\gamma}_0, b_\gamma\right)\right) \tag{48}$$

where Γ_{fv} is the designed diagonal matrix; $\tilde{\gamma}_0 > 0$ and $0 < b_\gamma < 1$ are the designed parameters.

$$\hat{\dot{\boldsymbol{\theta}}}_{fv} = \begin{cases} \Gamma_{fv}\boldsymbol{\omega}_{fv}\tilde{V}\mu(\left|\tilde{V}\right|) - \dfrac{(\hat{\boldsymbol{\theta}}_{fv}^{\mathrm{T}}\hat{\boldsymbol{\theta}}_{fv} - (\theta_{fv}^{\max})^2)^{n+1}}{2(\varepsilon_V^2 + 2\varepsilon_V\theta_{fv}^{\max})^{n+1}(\theta_{fv}^{\max})^2} \\ \cdot\left[\hat{\boldsymbol{\theta}}_{fv}^{\mathrm{T}}\Gamma_{fv}\boldsymbol{\omega}_{fv}\tilde{V}\mu(\left|\tilde{V}\right|) + \sqrt{(\hat{\boldsymbol{\theta}}_{fv}^{\mathrm{T}}\Gamma_{fv}\boldsymbol{\omega}_{fv}\tilde{V}\mu(\left|\tilde{V}\right|))^2 + \delta_V^2}\right]\hat{\boldsymbol{\theta}}_{fv}, & \left\|\hat{\boldsymbol{\theta}}_{fv}\right\|_2 > \theta_{fv}^{\max} \\ \Gamma_{fv}\boldsymbol{\omega}_{fv}\tilde{V}\mu(\left|\tilde{V}\right|), & \left\|\hat{\boldsymbol{\theta}}_{fv}\right\|_2 \le \theta_{fv}^{\max} \end{cases} \tag{45}$$

$$\dot{\hat{\boldsymbol{\theta}}}_{f\gamma} = \begin{cases} \Gamma_{f\gamma}\boldsymbol{\omega}_{f\gamma}\tilde{\gamma}\mu(|\tilde{\gamma}|) - \frac{(\hat{\boldsymbol{\theta}}_{f\gamma}^{\mathrm{T}}\hat{\boldsymbol{\theta}}_{f\gamma} - (\theta_{f\gamma}^{\max})^2)^{n+1}}{2(\varepsilon_{\gamma}^2 + 2\varepsilon_{\gamma}\theta_{f\gamma}^{\max})^{n+1}(\theta_{f\gamma}^{\max})^2} \\ \cdot \left[\hat{\boldsymbol{\theta}}_{f\gamma}^{\mathrm{T}}\Gamma_{f\gamma}\boldsymbol{\omega}_{f\gamma}\tilde{\gamma}\mu(|\tilde{\gamma}|) + \sqrt{(\hat{\boldsymbol{\theta}}_{f\gamma}^{\mathrm{T}}\Gamma_{f\gamma}\boldsymbol{\omega}_{f\gamma}\tilde{\gamma}\mu(|\tilde{\gamma}|))^2 + \delta_{\gamma}^2}\right]\hat{\boldsymbol{\theta}}_{f\gamma}, & \left\|\hat{\boldsymbol{\theta}}_{f\gamma}\right\|_2 > \theta_{f\gamma}^{\max} \\ \Gamma_{f\gamma}\boldsymbol{\omega}_{f\gamma}\tilde{\gamma}\mu(|\tilde{\gamma}|), & \left\|\hat{\boldsymbol{\theta}}_{f\gamma}\right\|_2 \le \theta_{f\gamma}^{\max} \end{cases} \tag{49}$$

$$\dot{\hat{\boldsymbol{\theta}}}_{fQ} = \begin{cases} \Gamma_{fQ}\boldsymbol{\omega}_{fQ}\tilde{Q}\mu(\left|\tilde{Q}\right|) - \frac{(\hat{\boldsymbol{\theta}}_{fQ}^{\mathrm{T}}\hat{\boldsymbol{\theta}}_{fQ} - (\theta_{fQ}^{\max})^2)^{n+1}}{2(\varepsilon_{Q}^2 + 2\varepsilon_{Q}\theta_{fQ}^{\max})^{n+1}(\theta_{fQ}^{\max})^2} \\ \cdot \left[\hat{\boldsymbol{\theta}}_{fQ}^{\mathrm{T}}\Gamma_{fQ}\boldsymbol{\omega}_{fQ}\tilde{Q}\mu(\left|\tilde{Q}\right|) + \sqrt{(\hat{\boldsymbol{\theta}}_{fQ}^{\mathrm{T}}\Gamma_{fQ}\boldsymbol{\omega}_{fQ}\tilde{Q}\mu(\left|\tilde{Q}\right|))^2 + \delta_{Q}^2}\right]\hat{\boldsymbol{\theta}}_{fQ}, & \left\|\hat{\boldsymbol{\theta}}_{fQ}\right\|_2 > \theta_{fQ}^{\max} \\ \Gamma_{fQ}\boldsymbol{\omega}_{fQ}\tilde{Q}\mu(\left|\tilde{Q}\right|), & \left\|\hat{\boldsymbol{\theta}}_{fQ}\right\|_2 \le \theta_{fQ}^{\max} \end{cases} \tag{55}$$

The above Eq. (48) is expanded to the following specific form (49), as shpwn at the top of this page, where ε_{γ}, δ_{γ}, and $\theta_{fQ}^{\max}$ are the designed parameters.

Step 2: Let θ_{d} and $\dot{\theta}_{\mathrm{d}}$ be the tracking and differential signals obtained by introducing the second-order filter [33] to process the virtual control law θ_c. Differentiating $\tilde{\theta}$ by time t, we have

$$\dot{\tilde{\theta}} = Q - \dot{\theta}_{\mathrm{d}}. \tag{50}$$

The virtual control law Q_c is designed as

$$Q_c = -k_{\theta 1}\tilde{\theta} - k_{\theta 2}\int_0^t \tilde{\theta}\mathrm{d}\tau - g_{\gamma}\tilde{\gamma} + \dot{\theta}_{\mathrm{d}}, \tag{51}$$

Step 3: Let Q_{d} and $\dot{Q}_{\mathrm{d}}$ be the tracking and differential signals obtained by introducing the second-order filter [33] to process the virtual control law Q_c. Differentiating $\tilde{Q}$ by time t, we have

$$\dot{\tilde{Q}} = g_Q\delta_{\mathrm{e}} + \boldsymbol{\omega}_{fQ}^{\mathrm{T}}\boldsymbol{\theta}_{fQ} - \dot{Q}_{\mathrm{d}}. \tag{52}$$

The control law δ_{e} is designed as

$$\delta_{\mathrm{e}} = g_Q^{-1}\left(-k_{Q1}\tilde{Q} - k_{Q2}\int_0^t \tilde{Q}\mathrm{d}\tau - \boldsymbol{\omega}_{fQ}^{\mathrm{T}}\hat{\boldsymbol{\theta}}_{fQ} - \tilde{\theta} + \dot{Q}_{\mathrm{d}}\right), \tag{53}$$

where $\hat{\boldsymbol{\theta}}_{fQ}$ is the estimated value of $\boldsymbol{\theta}_{fQ}$.

The adaptive law of $\hat{\boldsymbol{\theta}}_{fQ}$ is designed as

$$\dot{\hat{\boldsymbol{\theta}}}_{fQ} = \mathrm{Proj}(\hat{\boldsymbol{\theta}}_{fQ}, \Gamma_{fQ}\boldsymbol{\omega}_{fQ}\tilde{Q}\mu(\left|\tilde{Q}\right|, \tilde{Q}_0, b_Q)), \tag{54}$$

where Γ_{fQ} is the designed diagonal matrix; $\tilde{Q}_0 > 0$ and $0 < b_Q < 1$ are the designed parameters.

The Eq. (55) is rewritten as (55), as shown at the top of this page, where ε_Q, δ_Q, and $\theta_{fQ}^{\max}$ are the designed parameters.

For the close-loop system consisting of the controller and AHV model, the schematic diagram of control structure is summarized as Fig. 3.

3) STABILITY ANALYSIS

In this section, the stability of the designed controller is analyzed, and the following conclusion is drawn.

Theorem 1: Considering the close-loop system consisting of the AHV model (Eqs. (1)∼(7)), command transform (Eq. (9)), virtual control law(Eqs. (47), (51)), actual control law (Eqs. (40), (53)), adaptive law (Eqs. (45), (49), (55)), and the second-order filters, the tracking error $\tilde{V}$ and $\tilde{h}$ are bounded.

Proof: For the $V-subsystem$, the Lyapunov function is selected as

$$W_V = \frac{1}{2}\left(\tilde{V}^2 + k_{V2}\left(\int_0^t \tilde{V}\mathrm{d}\tau\right)^2 + \tilde{\boldsymbol{\theta}}_{fv}^{\mathrm{T}}\Gamma_{fv}^{-1}\tilde{\boldsymbol{\theta}}_{fv}\right), \tag{56}$$

where $\tilde{\boldsymbol{\theta}}_{fv} = \boldsymbol{\theta}_{fv} - \hat{\boldsymbol{\theta}}_{fv}$.

Substituting (40) into (39) yields

$$\begin{aligned} \dot{\tilde{V}} &= g_V\left[g_V^{-1}\left(-k_{V1}\tilde{V} - k_{V2}\int_0^t \tilde{V}\mathrm{d}\tau \right.\right. \\ &\quad \left.\left. -\boldsymbol{\omega}_{fv}^{\mathrm{T}}\hat{\boldsymbol{\theta}}_{fv} + g\sin\gamma + \dot{V}_{\mathrm{ref}}\right)\right] \\ &\quad +\boldsymbol{\omega}_{fv}^{\mathrm{T}}\boldsymbol{\theta}_{fv} - g\sin\gamma - \dot{V}_{\mathrm{ref}} \\ &= -k_{V1}\tilde{V} - k_{V2}\int_0^t \tilde{V}\mathrm{d}\tau + \boldsymbol{\omega}_{fv}^{\mathrm{T}}\tilde{\boldsymbol{\theta}}_{fv} \end{aligned} \tag{57}$$

Differentiating W_V by time t and invoking (57), we have

$$\begin{aligned} \dot{W}_V &= \tilde{V}\dot{\tilde{V}} + k_{V2}\tilde{V}\int_0^t \tilde{V}\mathrm{d}\tau - \tilde{\boldsymbol{\theta}}_{fv}^{\mathrm{T}}\Gamma_{fv}^{-1}\dot{\hat{\boldsymbol{\theta}}}_{fv} \\ &= \tilde{V}\left(-k_{V1}\tilde{V} - k_{V2}\int_0^t \tilde{V}\mathrm{d}\tau \right. \\ &\quad \left. +\boldsymbol{\omega}_{fv}^{\mathrm{T}}\tilde{\boldsymbol{\theta}}_{fv}\right) + k_{V2}\tilde{V}\int_0^t \tilde{V}\mathrm{d}\tau - \tilde{\boldsymbol{\theta}}_{fv}^{\mathrm{T}}\Gamma_{fv}^{-1}\dot{\hat{\boldsymbol{\theta}}}_{fv} \\ &= -k_{V1}\tilde{V}^2 - \tilde{\boldsymbol{\theta}}_{fv}^{\mathrm{T}}(\Gamma_{fv}^{-1}\dot{\hat{\boldsymbol{\theta}}}_{fv} - \tilde{V}\boldsymbol{\omega}_{fv}) \end{aligned} \tag{58}$$

Substituting (44) into (58) yields

$$\begin{aligned} \dot{W}_V &= -k_{V1}\tilde{V}^2 - \tilde{\boldsymbol{\theta}}_{fv}^{\mathrm{T}} \\ &\quad \times\left[\Gamma_{fv}^{-1}\mathrm{Proj}(\hat{\boldsymbol{\theta}}_{fv}, \Gamma_{fv}\boldsymbol{\omega}_{fv}\tilde{V}\mu(\left|\tilde{V}\right|, \tilde{V}_0, b_V)) - \tilde{V}\boldsymbol{\omega}_{fv}\right] \end{aligned} \tag{59}$$

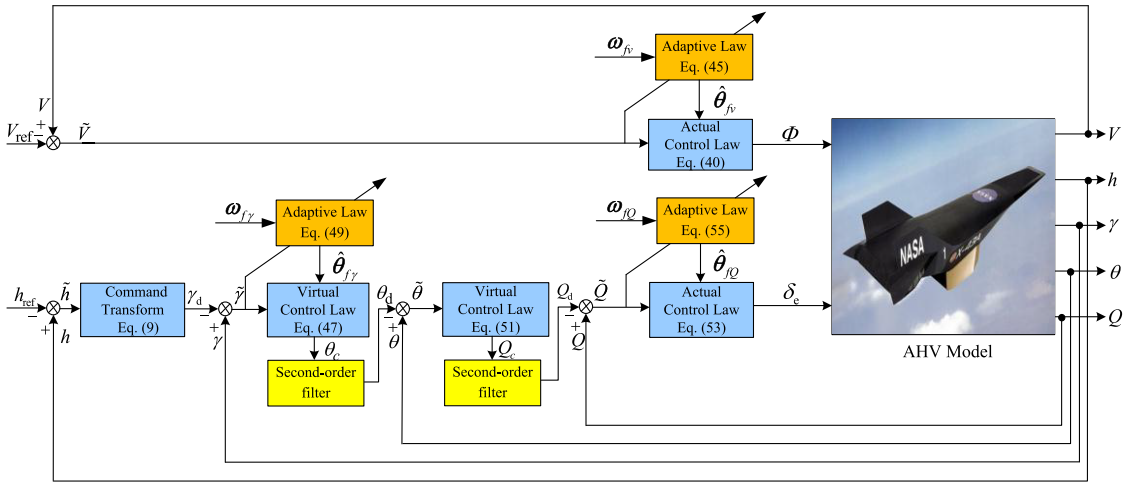

FIGURE 3. Structure of the close-loop system consisting of the controller and AHV model.

According to the property of the projective operator [28], the following inequality holds.

$$\tilde{\boldsymbol{\theta}}_{fv}^{\mathrm{T}}\mathrm{Proj}(\hat{\boldsymbol{\theta}}_{fv}, \Gamma_{fv}\boldsymbol{\omega}_{fv}\tilde{V}\mu(\left|\tilde{V}\right|, \tilde{V}_0, b_V)) \geq \tilde{\boldsymbol{\theta}}_{fv}^{\mathrm{T}}\Gamma_{fv}\boldsymbol{\omega}_{fv}\tilde{V}\mu(\left|\tilde{V}\right|, \tilde{V}_0, b_V) \quad (60)$$

Thus, we have

$$\begin{aligned}\dot{W}_V &\leq -k_{V1}\tilde{V}^2 - \tilde{\boldsymbol{\theta}}_{fv}^{\mathrm{T}}(\Gamma_{fv}^{-1}\Gamma_{fv}\boldsymbol{\omega}_{fv}\tilde{V}\mu(\left|\tilde{V}\right|, \tilde{V}_0, b_V) - \tilde{V}\boldsymbol{\omega}_{fv}) \\ &= -k_{V1}\tilde{V}^2 - \tilde{\boldsymbol{\theta}}_{fv}^{\mathrm{T}}\tilde{V}\boldsymbol{\omega}_{fv}(\mu(\left|\tilde{V}\right|, \tilde{V}_0, b_V) - 1) \quad (61)\end{aligned}$$

If $\left|\tilde{V}\right| \geq \tilde{V}_0$, according to the definition of the Lipschitz continuous dead-zone modification described as the Eq. (42), we have $\mu(\left|\tilde{V}\right|, \tilde{V}_0, b_V) = 1$. Thus,

$$-\tilde{\boldsymbol{\theta}}_{fv}^{\mathrm{T}}\tilde{V}\boldsymbol{\omega}_{fv}(\mu(\left|\tilde{V}\right|, \tilde{V}_0, b_V) - 1) = 0. \quad (62)$$

If $\left|\tilde{V}\right| < \tilde{V}_0$, we have $0 \leq \mu(\left|\tilde{V}\right|, \tilde{V}_0, b_V) < 1$. Assuming that there is a positive constant $\bar{f}_v$ such that $\left|\boldsymbol{\omega}_{fv}^{\mathrm{T}}\tilde{\boldsymbol{\theta}}_{fv}\right| \leq \bar{f}_v$ holds, we obtain the following inequality:

$$\begin{aligned}&-\tilde{\boldsymbol{\theta}}_{fv}^{\mathrm{T}}\tilde{V}\boldsymbol{\omega}_{fv}(\mu(\left|\tilde{V}\right|, \tilde{V}_0, b_V) - 1) \\ &\quad \leq \left|\tilde{V}\right| \cdot \left|\tilde{\boldsymbol{\theta}}_{fv}^{\mathrm{T}}\boldsymbol{\omega}_{fv}\right| \cdot \left|\mu(\left|\tilde{V}\right|, \tilde{V}_0, b_V) - 1\right| \leq \tilde{V}_0\bar{f}_v. \quad (63)\end{aligned}$$

Combining (62), (63) with (61), we obtain

$$\dot{W}_V \leq -k_{V1}\tilde{V}^2 + \tilde{V}_0\bar{f}_v. \quad (64)$$

For the $h-$ *subsystem*, substituting (47) into (46) yields

$$\begin{aligned}\dot{\tilde{\gamma}} &= g_\gamma\,(\theta - \theta_{\mathrm{d}} + \theta_{\mathrm{d}} - \theta_{\mathrm{c}} + \theta_{\mathrm{c}}) + \boldsymbol{\omega}_{f\gamma}^{\mathrm{T}}\boldsymbol{\theta}_{f\gamma} - \frac{g}{V}\cos\gamma - \dot{\gamma}_{\mathrm{d}} \\ &= g_\gamma\left(\tilde{\theta} + y_1 + \theta_{\mathrm{c}}\right) + \boldsymbol{\omega}_{f\gamma}^{\mathrm{T}}\boldsymbol{\theta}_{f\gamma} - \frac{g}{V}\cos\gamma - \dot{\gamma}_{\mathrm{d}} \\ &= -k_{\gamma 1}\tilde{\gamma} - k_{\gamma 2}\int_0^t \tilde{\gamma}\mathrm{d}\tau + \boldsymbol{\omega}_{f\gamma}^{\mathrm{T}}\tilde{\boldsymbol{\theta}}_{f\gamma} + g_\gamma\tilde{\theta} + g_\gamma y_1 \quad (65)\end{aligned}$$

where $\tilde{\boldsymbol{\theta}}_{f\gamma} = \boldsymbol{\theta}_{f\gamma} - \hat{\boldsymbol{\theta}}_{f\gamma}$.

Similarly, we obtain the following equalities:

$$\begin{aligned}\dot{\tilde{\theta}} &= Q - Q_{\mathrm{d}} + Q_{\mathrm{d}} - Q_{\mathrm{c}} + Q_{\mathrm{c}} - \dot{\theta}_{\mathrm{d}} \\ &= \tilde{Q} + y_2 + Q_{\mathrm{c}} - \dot{\theta}_{\mathrm{d}} \\ &= -k_{\theta 1}\tilde{\theta} - k_{\theta 2}\int_0^t \tilde{\theta}\mathrm{d}\tau - g_\gamma\tilde{\gamma} + \tilde{Q} + y_2 \quad (66)\end{aligned}$$

$$\begin{aligned}\dot{\tilde{Q}} &= g_Q g_Q^{-1}\left(-k_{Q1}\tilde{Q} - k_{Q2}\int_0^t \tilde{Q}\mathrm{d}\tau\right. \\ &\quad \left. - \boldsymbol{\omega}_{fQ}^{\mathrm{T}}\hat{\boldsymbol{\theta}}_{fQ} - \tilde{\theta} + \dot{Q}_{\mathrm{d}}\right) + \boldsymbol{\omega}_{fQ}^{\mathrm{T}}\boldsymbol{\theta}_{fQ} - \dot{Q}_{\mathrm{d}} \\ &= -k_{Q1}\tilde{Q} - k_{Q2}\int_0^t \tilde{Q}\mathrm{d}\tau + \boldsymbol{\omega}_{fQ}^{\mathrm{T}}\tilde{\boldsymbol{\theta}}_{fQ} - \tilde{\theta} \quad (67)\end{aligned}$$

where $\tilde{\boldsymbol{\theta}}_{fQ} = \boldsymbol{\theta}_{fQ} - \hat{\boldsymbol{\theta}}_{fQ}$.

Select the following Lyapunov function (68), as shown at the top of the next page.

Differentiating W_h by time t and invoking (65)∼(67), we have

$$\begin{aligned}\dot{W}_h = &-k_{\gamma 1}\tilde{\gamma}^2 - k_{\theta 1}\tilde{\theta}^2 - k_{Q1}\tilde{Q}^2 + g_\gamma y_1\tilde{\gamma} + y_2\tilde{\theta} \\ &-\tilde{\boldsymbol{\theta}}_{f\gamma}^{\mathrm{T}}(\Gamma_{f\gamma}^{-1}\dot{\hat{\boldsymbol{\theta}}}_{f\gamma} - \tilde{\gamma}\boldsymbol{\omega}_{f\gamma}) - \tilde{\boldsymbol{\theta}}_{fQ}^{\mathrm{T}}(\Gamma_{fQ}^{-1}\dot{\hat{\boldsymbol{\theta}}}_{fQ} - \tilde{Q}\boldsymbol{\omega}_{fQ}) \quad (69)\end{aligned}$$

Since

$$g_\gamma y_1\tilde{\gamma} \leq |g_\gamma|\,|y_1\tilde{\gamma}| \leq |g_\gamma|\left(\frac{\bar{y}_1^2}{2} + \frac{\tilde{\gamma}^2}{2}\right), \quad (70)$$

$$y_2\tilde{\theta} \leq \frac{\bar{y}_2^2}{2} + \frac{\tilde{\theta}^2}{2}, \quad (71)$$

we obtain the inequality as follows:

$$\begin{aligned}\dot{W}_h \leq &-\left(k_{\gamma 1} - \frac{|g_\gamma|}{2}\right)\tilde{\gamma}^2 - \left(k_{\theta 1} - \frac{1}{2}\right)\tilde{\theta}^2 \\ &- k_{Q1}\tilde{Q}^2 + \frac{|g_\gamma|\,\bar{y}_1^2}{2} + \frac{\bar{y}_2^2}{2} - \tilde{\boldsymbol{\theta}}_{f\gamma}^{\mathrm{T}}(\Gamma_{f\gamma}^{-1}\dot{\hat{\boldsymbol{\theta}}}_{f\gamma} \\ &- \tilde{\gamma}\boldsymbol{\omega}_{f\gamma}) - \tilde{\boldsymbol{\theta}}_{fQ}^{\mathrm{T}}(\Gamma_{fQ}^{-1}\dot{\hat{\boldsymbol{\theta}}}_{fQ} - \tilde{Q}\boldsymbol{\omega}_{fQ}) \quad (72)\end{aligned}$$

$$W_h = \frac{1}{2}\begin{pmatrix} \tilde{\gamma}^2 + k_{\gamma 2}\left(\int_0^t \tilde{\gamma}\mathrm{d}\tau\right)^2 + \tilde{\theta}^2 + k_{\theta 2}\left(\int_0^t \tilde{\theta}\mathrm{d}\tau\right)^2 + \tilde{Q}^2 \\ +k_{Q2}\left(\int_0^t \tilde{Q}\mathrm{d}\tau\right)^2 + \tilde{\boldsymbol{\theta}}_{f\gamma}^{\mathrm{T}}\Gamma_{f\gamma}^{-1}\tilde{\boldsymbol{\theta}}_{f\gamma} + \tilde{\boldsymbol{\theta}}_{fQ}^{\mathrm{T}}\Gamma_{fQ}^{-1}\tilde{\boldsymbol{\theta}}_{fQ} \end{pmatrix}. \tag{68}$$

Substituting (48),(54) into (72) and using the property of the projective operator [28], we have

$$\begin{aligned} \dot{W}_h \leq & -\left(k_{\gamma 1} - \frac{|g_\gamma|}{2}\right)\tilde{\gamma}^2 - \left(k_{\theta 1} - \frac{1}{2}\right)\tilde{\theta}^2 - k_{Q1}\tilde{Q}^2 \\ & + \frac{|g_\gamma|\bar{y}_1^2}{2} + \frac{\bar{y}_2^2}{2} - \tilde{\boldsymbol{\theta}}_{f\gamma}^{\mathrm{T}}\tilde{\gamma}\boldsymbol{\omega}_{f\gamma}(\mu(|\tilde{\gamma}|, \tilde{\gamma}_0, b_\gamma) - 1) \\ & - \tilde{\boldsymbol{\theta}}_{fQ}^{\mathrm{T}}\tilde{Q}\boldsymbol{\omega}_{fQ}(\mu(\left|\tilde{Q}\right|, \tilde{Q}_0, b_Q) - 1) \end{aligned} \tag{73}$$

Assume that there is a positive constant $\bar{f}_\gamma$ and $\bar{f}_Q$ such that $\left|\boldsymbol{\omega}_{f\gamma}^{\mathrm{T}}\tilde{\boldsymbol{\theta}}_{f\gamma}\right| \leq \bar{f}_\gamma$ and $\left|\boldsymbol{\omega}_{fQ}^{\mathrm{T}}\tilde{\boldsymbol{\theta}}_{fQ}\right| \leq \bar{f}_Q$ hold. Similar to the analytical derivation process described as Eqs. (61)∼(64), we obtain the following inequality

$$\dot{W}_h \leq -\left(k_{\gamma 1} - \frac{|g_\gamma|}{2}\right)\tilde{\gamma}^2 - \left(k_{\theta 1} - \frac{1}{2}\right)\tilde{\theta}^2 - k_{Q1}\tilde{Q}^2 + M, \tag{74}$$

where $M = \frac{|g_\gamma|\bar{y}_1^2}{2} + \frac{\bar{y}_2^2}{2} + \bar{f}_\gamma\tilde{\gamma}_0 + \bar{f}_Q\tilde{Q}_0$.

Choosing $k_{\gamma 1} > |g_\gamma|/2$ and $k_{\theta 1} > 1/2$, the compact sets are defined as

$$\begin{cases} \Omega_{\tilde{V}} = \left\{\tilde{V} \middle| \left|\tilde{V}\right| \leq \sqrt{\tilde{V}_0\bar{f}_v / k_{V1}}\right\} \\ \Omega_{\tilde{\gamma}} = \left\{\tilde{\gamma} \middle| |\tilde{\gamma}| \leq \sqrt{M \Big/ \left(k_{\gamma 1} - \frac{|g_\gamma|}{2}\right)}\right\} \\ \Omega_{\tilde{\theta}} = \left\{\tilde{\theta} \middle| \left|\tilde{\theta}\right| \leq \sqrt{M \Big/ \left(k_{\theta 1} - \frac{1}{2}\right)}\right\} \\ \Omega_{\tilde{Q}} = \left\{\tilde{Q} \middle| \left|\tilde{Q}\right| \leq \sqrt{M / k_{Q1}}\right\} \end{cases} \tag{75}$$

The radiuses of compact sets described as Eq. (75) can be arbitrarily small by selecting enough largek_{V1}, $k_{\gamma 1}$, $k_{\theta 1}$ and k_{Q1}. The inequalities $\dot{W}_V < 0$ holds for $\tilde{V} \neq 0$, and $\dot{W}_h < 0$ holds when the tracking error is not within compact sets described as Eq. (75). According to the Lyapunov theory, the tracking error $\tilde{V}$ and $\tilde{\gamma}$ are bounded. Furthermore, we obtain that$\tilde{h}$ is bounded [32]. □

IV. SIMULATIONS

This section aims to verify the performance of the proposed robust controller with an adaptive projection-based parameter estimator. Firstly, the simulation on the nominal controller presented in Section III.A is carried out to verify the effectiveness of the designed control framework. Then, the robustness of the proposed robust controller described in Section III.B is verified.

A. PERFORMANCE OF THE NOMINAL CONTROLLER

The model parameters, and the coefficients of aerodynamic forces and thrust are given in Table 2-6. Firstly, the AHV model is trimmed at the initial time. The initial flight state is selected to maintain horizontal flight at the height of 25,908 m and the velocity of 2,347 m/s. The values of the initial states are given in Table 1.

TABLE 1. States initialization.

State/Units	Value	State/Units	Value
V /(m/s)	2347	$\dot{\eta}_1$	0
h /m	25908	η_2	0.33492
γ /(°)	0	$\dot{\eta}_2$	0
θ /(°)	1.5318	Φ	0.0849
Q /(°)	0	δ_e /(°)	4.5805
η_1	0.93815		

The reference commands $\mathbf{y}_{ref} = [V_{ref}, h_{ref}]$ are selected as follows: the velocity steps 100 m/s per 50 s, and the altitude changes with a square wave (the amplitude is 300 m and period 100 s). The reference commands are generated by the filter as follows [27]:

$$\frac{h_{\mathrm{ref}}(s)}{h_{\mathrm{c}}(s)} = \frac{V_{\mathrm{ref}}(s)}{V_{\mathrm{c}}(s)} = \left(\frac{\omega_A^2}{s^2 + 2\zeta_A\omega_A s + \omega_A^2}\right)^2, \tag{76}$$

where ζ_A and ω_A are the designed parameters.

Choose the PI coefficients as follows: $k_{V1} = 1.8$, $k_{V2} = 0.5$, $k = 0.6$, $k_{\mathrm{I}} = 0.1$, $k_{\gamma 1} = 2$, $k_{\gamma 2} = 0.2$, $k_{\theta 1} = 3$, $k_{\theta 2} = 0.2$, $k_{Q1} = 4$, $k_{Q2} = 0.2$. Parameters for the reference command filter are selected as: $\zeta_A = 0.95$, $\omega_A = 0.4$. The simulation time is taken as 150 s, and the differential equations are solved by Runge-Kutta method with the step 0.01s. The simulation results are depicted in the Figs. 4∼6.

Fig. 4 shows the tracking performance of the velocity and altitude by the nominal controller. It can be seen that the nominal controller achieves stable tracking of the reference commands, and the tracking error is kept in a small range. The magnitude of the velocity tracking error shown in Fig. 4(c) is extremely small. This phenomenon can be explained by the following two aspects. Firstly, by analyzing the design process of the nominal controller, it can be concluded that the $V-subsystem$ is a first-order dynamic system wherein there are no accumulation of errors caused by the filters. Secondly, under the nominal conditions, the model used in the simulation is accurately known, without considering the model

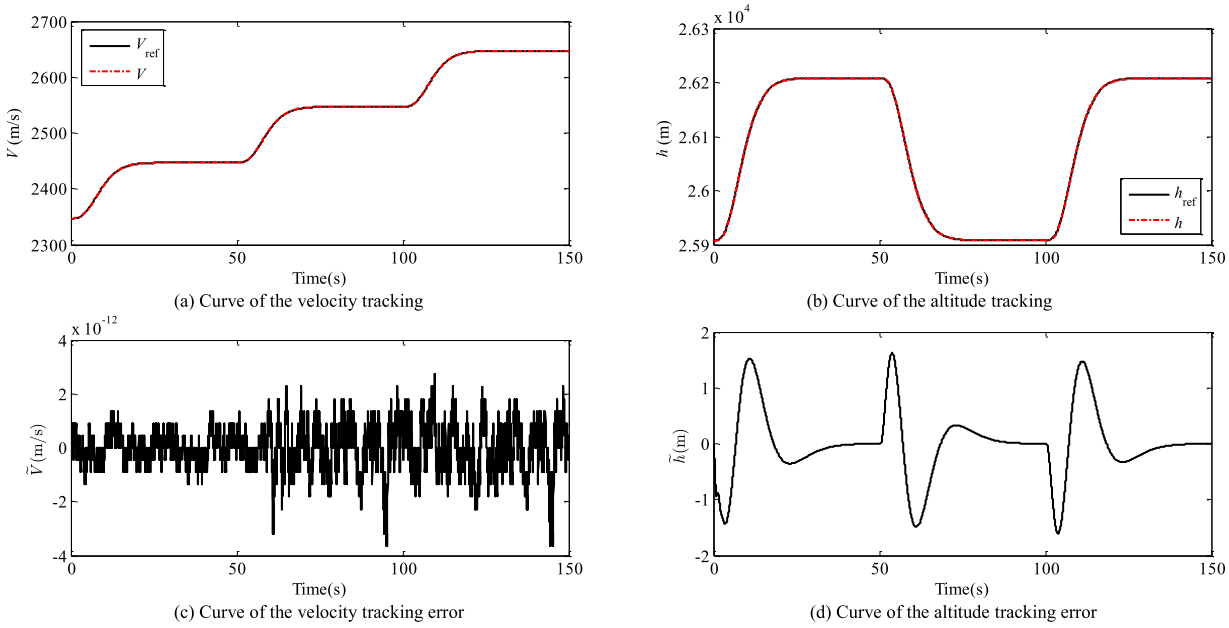

FIGURE 4. Tracking performance of the velocity and altitude by the nominal controller.

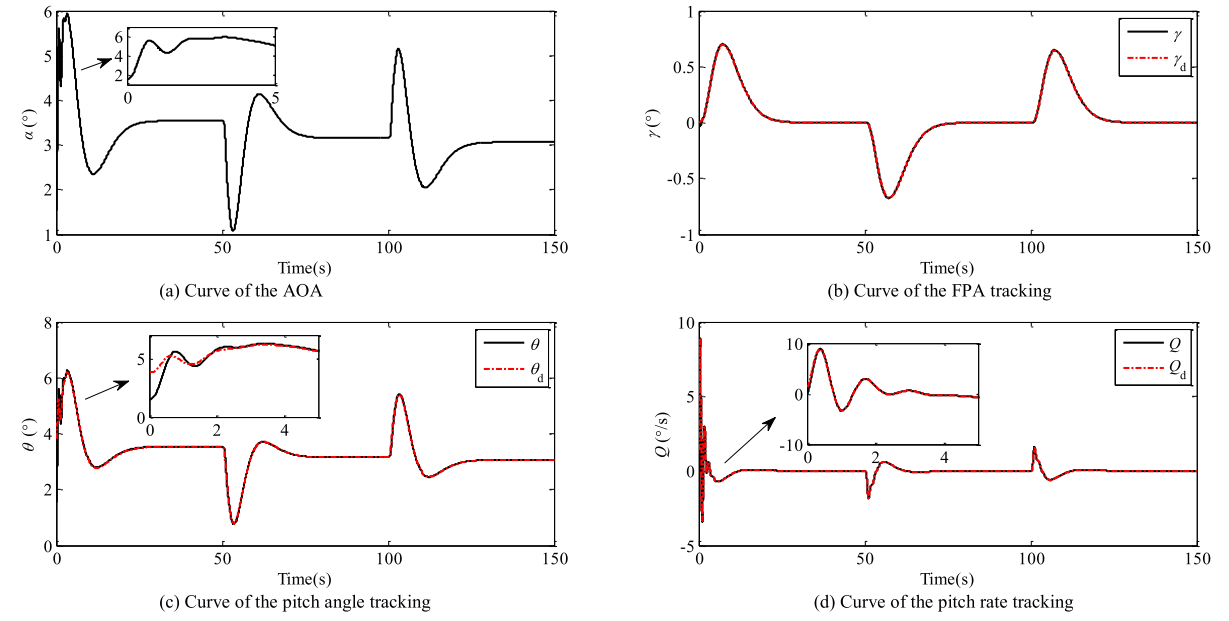

FIGURE 5. Curves of the rigid states by the nominal controller.

uncertainty and the flexible states. Thus, the phenomenon shown in Fig. 4(c) is reasonable.

Next, we analyze the characteristics of the rigid states. As shown in Fig. 5(a), the angle of attack is within a reasonable range, namely $\alpha \in (1°, 6°)$, which meets the demand of intaking air for the scramjet. Figs. 5(b)∼(d) indicate that the flight path angle, pitch angle and pitch rate steadily track their commands and remain within a reasonable range. The curves of the rigid states change smoothly and no phenomenon of the high frequency chattering occurs. Finally, the performance of the control inputs is analyzed. As shown in Fig. 6, the fuel equivalence ratio and the elevator deflection change smoothly within a executable range, and no high frequency chattering is observed. It can be seen from Fig. 6(b) that the value of elevator deflection sharply fluctuates in the initial period, which is harmful for the stable control. However, from the magnified view of the elevator deflection curve in $(0, 5s)$, we can conclude that the amplitude and frequency of the fluctuation are within a reasonable range, and the fluctuation gradually disappears within 2s. To sum up, we conclude that under

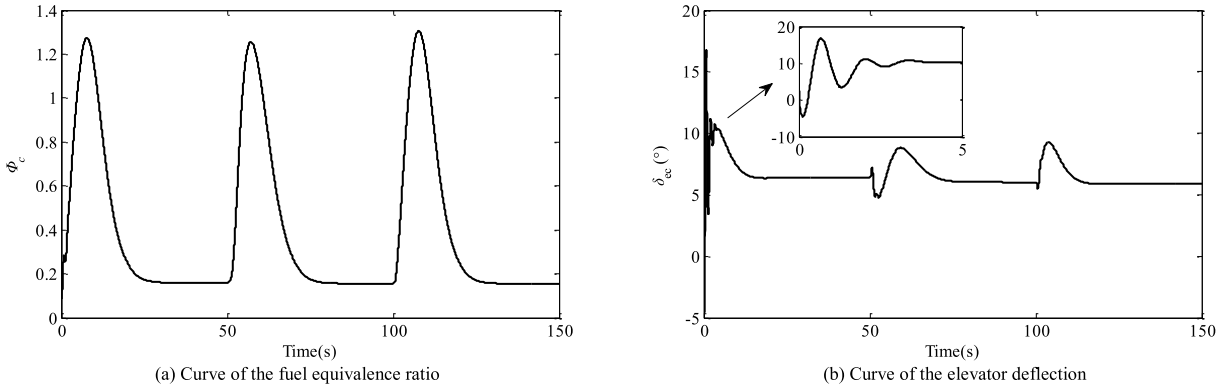

(a) Curve of the fuel equivalence ratio (b) Curve of the elevator deflection

FIGURE 6. Curve of the control inputs by the nominal controller.

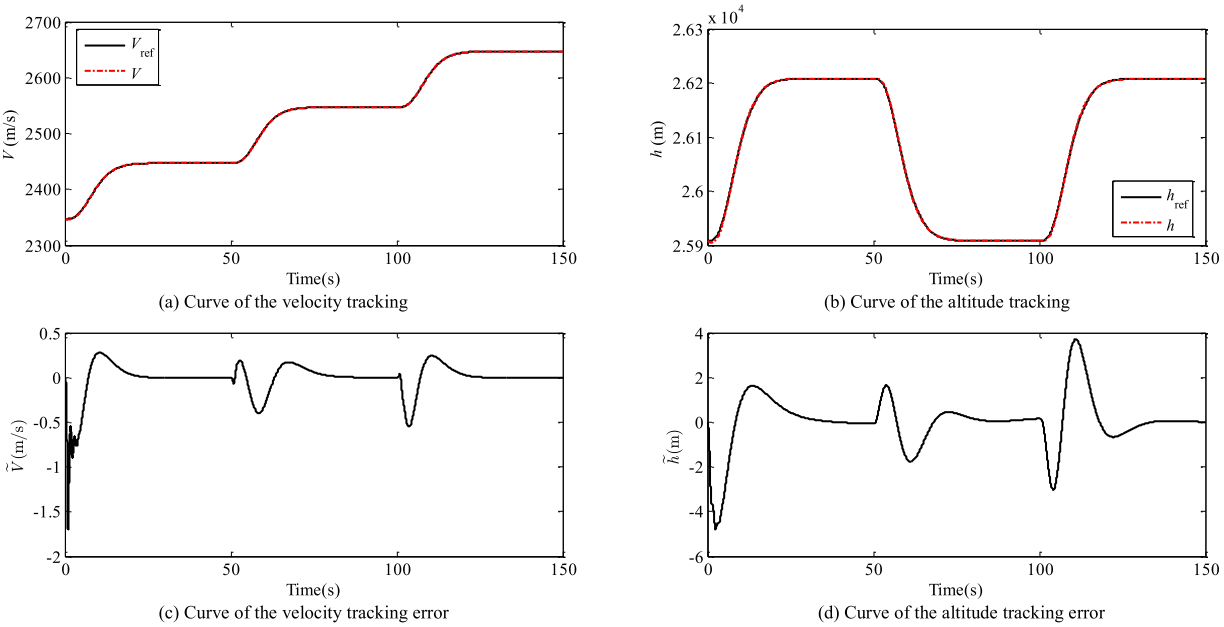

(a) Curve of the velocity tracking (b) Curve of the altitude tracking

(c) Curve of the velocity tracking error (d) Curve of the altitude tracking error

FIGURE 7. Tracking performance of the velocity and altitude by the proposed robust controller.

nominal conditions, the designed nominal controller achieved the stable tracking of reference commands with a satisfactory performance.

B. PERFORMANCE OF THE PROPOSED ROBUST CONTROLLER

The model used in this section is consistent with the previous section in the selection of model parameters, initial trim points, and reference commands. To verify the robustness of the proposed controller, the flexible states are taken into account. The constants of aero-propulsive coupling are selected as: $\tilde{\psi}_1 = 147.9298$, $\tilde{\psi}_2 = 109.5250$. Moreover, the parameter perturbations are added to the aerodynamic coefficients and thrust coefficients of the AHV model. The maximum amplitude and the frequency of the perturbation are selected as $A = 30\%$, $\omega = 0.01\pi \,\mathrm{rad} \cdot \mathrm{s}^{-1}$.

The PI coefficients of the controller, filter parameters for virtual control law, and the simulation condition are selected to be the same as the Section IV.B. As for the parameter estimator, the parameters of adaptive laws are selected as follows: $\Gamma_{fv} = \mathrm{diag}(10^{-3}, 10^{-3}, 10^{-4}, 10^{-6}, 10^{-2}, 10^{-4}, 10^{-5})$, $\Gamma_{f\gamma} = \mathrm{diag}(10^{-2}, 10^{-3}, 10^{-3}, 10^{-4}, 10^{-3}, 10^{-3}, 10^{-4}, 10^{-6}, 10^{-2}, 10^{-5})$, $\Gamma_{fQ} = \mathrm{diag}(10^{-4}, 10^{-5}, 10^{-5}, 10^{-6}, 10^{-5}, 10^{-4}, 10^{-5}, 10^{-6})$; $\tilde{V}_0 = 5 \times 10^{-5}$, $\tilde{\gamma}_0 = 5 \times 10^{-4}$, $\tilde{Q}_0 = 5 \times 10^{-3}$, $b_V = 0.5$, $b_\gamma = 0.5$, $b_Q = 0.5$, $\theta_{fv}^{\max} = 2.01 \times 10^{-2}$, $\varepsilon_V = 10^{-4}$, $\delta_V = 10^{-4}$, $\theta_{f\gamma}^{\max}$=4.0571 $\times 10^{-2}$, $\varepsilon_\gamma = 10^{-4}$, $\delta_\gamma = 10^{-4}$, $\theta_{fQ}^{\max} = 2.87 \times 10^{-4}$, $\varepsilon_Q = 10^{-6}$, $\delta_Q = 10^{-6}$. The simulation results are depicted in the Figs. 7∼10.

It can be seen from Fig. 7 that the proposed controller achieves the stable tracking of reference commands. The velocity tracking error is kept in $(-2, 2)$ m $\cdot$ s^{-1}, and the altitude tracking error kept in $(-5, 5)$ m. Fig. 8 shows that the

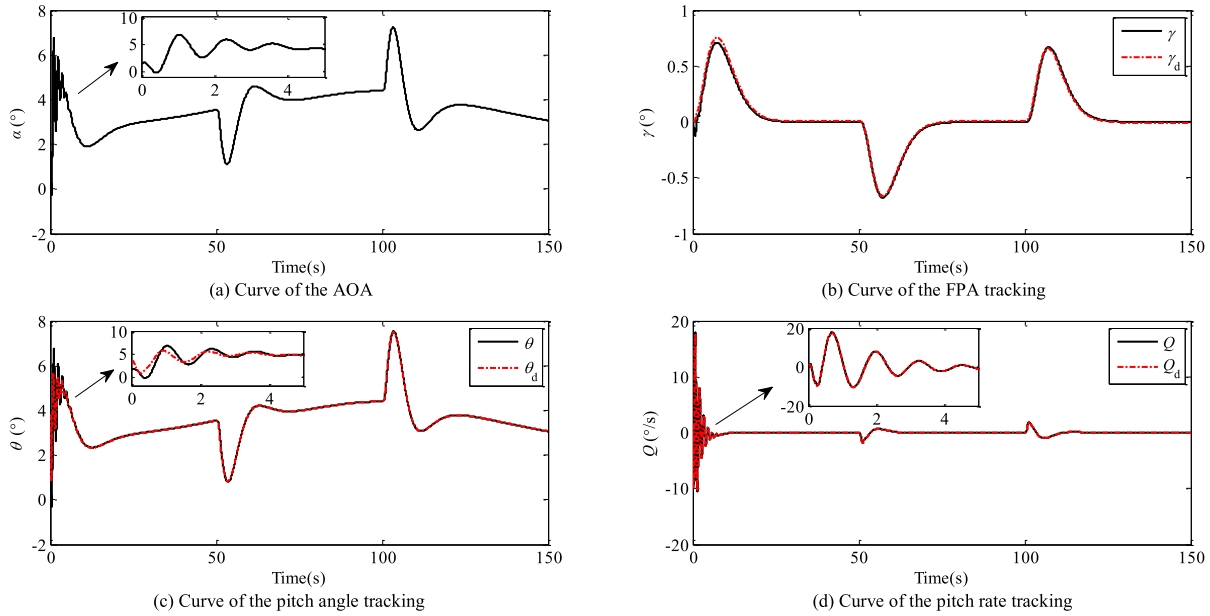

(a) Curve of the AOA
(b) Curve of the FPA tracking
(c) Curve of the pitch angle tracking
(d) Curve of the pitch rate tracking

FIGURE 8. Curves of the rigid states by the proposed robust controller.

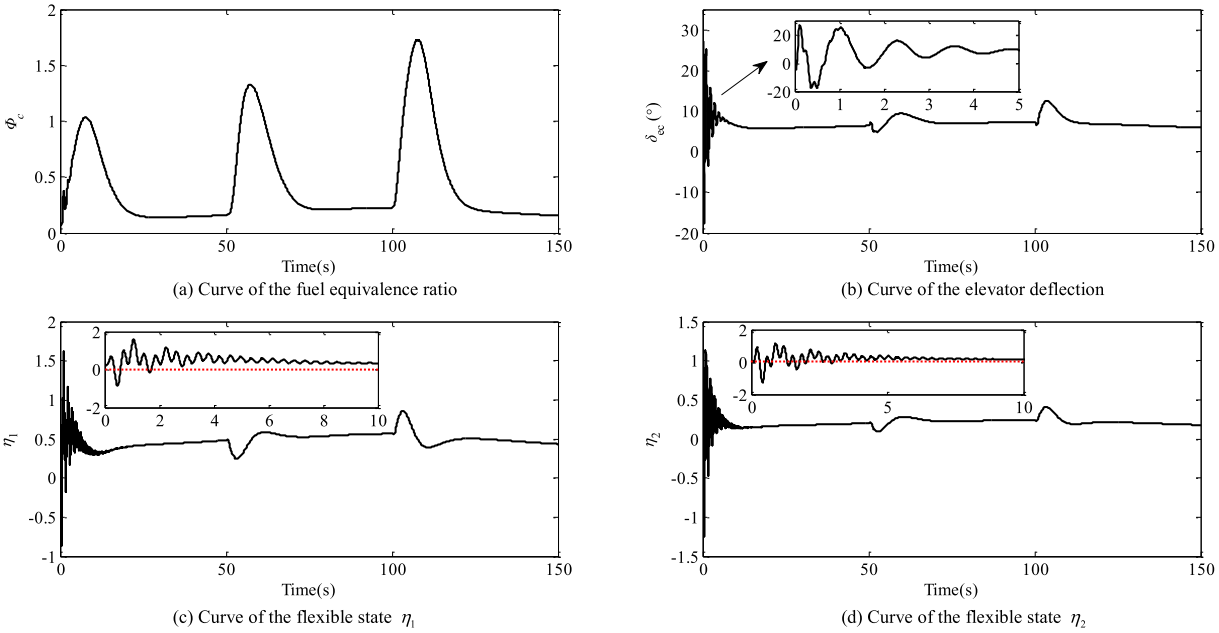

(a) Curve of the fuel equivalence ratio
(b) Curve of the elevator deflection
(c) Curve of the flexible state η_1
(d) Curve of the flexible state η_2

FIGURE 9. Curves of the control inputs and the flexible states by the proposed robust controller.

rigid states change smoothly within a reasonable range, and the flight path angle, pitch angle and pitch rate steadily track their own commands. Figs. 9(a)∼(b) indicate that the control inputs change smoothly with a satisfactory performance. Compared with the control inputs by the nominal controller, the elevator deflection by the robust controller, depicted in the Fig. 9(b), has stronger chattering in the first five seconds. The chattering is mainly caused by the flexible states and the parameter perturbation. Figs. 9(c)∼(d) show that the flexible states chatter with a reasonable amplitude and frequency. The chattering of the flexible states is concentrated in the initial time, which is directly related to the chattering of the elevator deflection. The flexible state η_1 shows stronger chattering than the flexible state η_2, because the forebody of the AHV is slenderer and flatter than the aftbody. Fig. 10 shows the curves of the 2-norm of the variable parameters. It can be concluded that the variable parameters are limited within the preset range. To sum up, the proposed robust controller

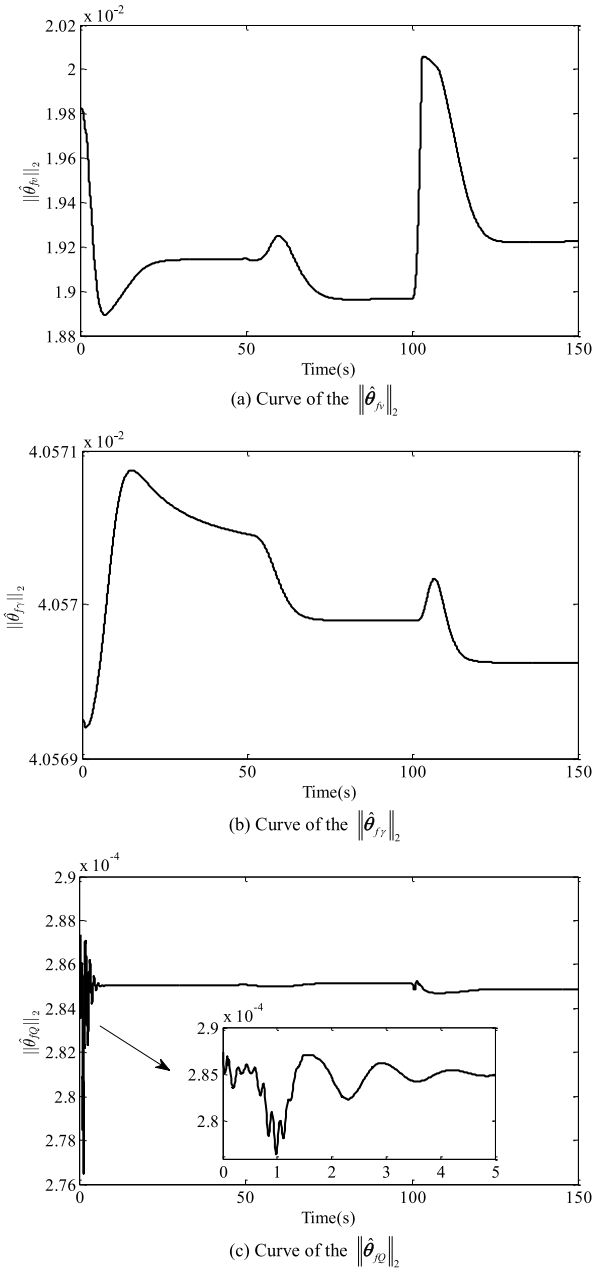

(a) Curve of the $\|\hat{\theta}_{fv}\|_2$

(b) Curve of the $\|\hat{\theta}_{f\gamma}\|_2$

(c) Curve of the $\|\hat{\theta}_{fQ}\|_2$

FIGURE 10. Curves for the 2-norm of the adaptive parameters.

achieved the stable tracking of the reference commands under the parameter perturbation, and the variable parameters are limited within the preset range.

V. CONCLUSION

A robust backstepping controller is presented for the air-breathing hypersonic vehicle in this paper. Compared with the previous studies, a novel parameter-varying model with fewer variable parameters is established, avoiding the problem of overparameterization and simplifying the controller design procedure. Furthermore, an adaptive parameter estimator combining the Lipschitz continuous dead-zone modification and the sufficiently smooth projection operator is designed, resulting in the uniform boundedness of adaptive parameters. In this way, the saturation of integrator can be avoided when

TABLE 2. Miscellaneous coefficient values.

Coefficient	Value	Units
S	3.0480×10^{1}	$m^2\cdot m^{-1}$
ρ_0	3.48×10^{-2}	$kg\cdot m^{-3}$
h_0	2.5908×10^{4}	m
h_s	6.5100×10^{3}	m
m	1.44×10^{4}	$kg\cdot m^{-1}$
I_{yy}	2.22×10^{6}	$kg\cdot m^2 / m$

TABLE 3. Lift and drag coefficient values.

Coefficient	Value	Units
C_L^{α}	4.6773×10^{0}	rad^{-1}
$C_T^{\delta_e}$	7.6224×10^{-1}	rad^{-1}
C_L^{0}	-1.8714×10^{-2}	–
$C_D^{\alpha^2}$	5.8224×10^{0}	rad^{-2}
C_D^{α}	-4.5315×10^{-2}	rad^{-1}
$C_D^{\delta_e^2}$	8.1993×10^{-1}	rad^{-2}
$C_D^{\delta_e}$	2.7669×10^{-4}	rad^{-1}
C_D^{0}	1.0131×10^{-2}	–

TABLE 4. Moment coefficient values.

Coefficient	Value	Units
z_T	2.5481×10^{0}	m
$\bar{c}$	5.1820×10^{0}	m
$C_{M,\alpha}^{\alpha^2}$	6.2926×10^{0}	rad^{-2}
$C_{M,\alpha}^{\alpha}$	2.1335×10^{0}	rad^{-1}
$C_{M,\alpha}^{0}$	1.8979×10^{-1}	–
c_e	-1.2897×10^{0}	rad^{-1}

TABLE 5. Thrust coefficient values.

Coefficient	Value	Units
β_1	-5.6083×10^{5}	$kg\cdot m^{-1}\cdot rad^{-3}$
β_2	-5.5387×10^{4}	$kg\cdot m^{-1}\cdot rad^{-3}$
β_3	3.9897×10^{4}	$kg\cdot m^{-1}\cdot rad^{-2}$
β_4	-2.5706×10^{4}	$kg\cdot m^{-1}\cdot rad^{-2}$
β_5	5.2883×10^{4}	$kg\cdot m^{-1}\cdot rad^{-1}$
β_6	-3.6031×10^{3}	$kg\cdot m^{-1}\cdot rad^{-1}$
β_7	9.4906×10^{3}	$kg\cdot m^{-1}$
β_8	-1.5013×10^{2}	$kg\cdot m^{-1}$

TABLE 6. N_1 and N_2 coefficient values.

Coefficient	Value	Units
$N_1^{\alpha^2}$	7.9649×10^{3}	$kg\bullet m^{-1}\bullet kg^{-0.5}\bullet rad^{-2}$
N_1^{α}	2.5997×10^{3}	$kg\bullet m^{-1}\bullet kg^{-0.5}\bullet rad^{-1}$
$N_1^{\delta_e}$	0.0000×10^{1}	$kg\bullet m^{-1}\bullet kg^{-0.5}\bullet rad^{-1}$
N_1^{0}	6.6797×10^{3}	$kg\bullet m^{-1}\bullet kg^{-0.5}$
$N_2^{\alpha^2}$	-2.8549×10^{4}	$kg\bullet m^{-1}\bullet kg^{-0.5}\bullet rad^{-2}$
N_2^{α}	1.6275×10^{4}	$kg\bullet m^{-1}\bullet kg^{-0.5}\bullet rad^{-1}$
$N_2^{\delta_e}$	7.0850×10^{3}	$kg\bullet m^{-1}\bullet kg^{-0.5}\bullet rad^{-1}$
N_2^{0}	-2.5123×10^{2}	$kg\bullet m^{-1}\bullet kg^{-0.5}$

the proposed controller is implemented in engineering. The robustness and effectiveness of the proposed controller is verified by the numerical simulation.

VI. APPENDIX

The model parameters, and the coefficients of aerodynamic forces and thrust are given in the following Table 2-6 [29], [30].

REFERENCES

[1] J. Tian, S. Zhang, Y. Zhang, and T. Li, "Active disturbance rejection control based robust output feedback autopilot design for airbreathing hypersonic vehicles," *ISA Trans.*, vol. 74, pp. 45–59, Mar. 2018.
[2] K. Sachan and R. Padhi, "A brief survey on six-degree-of-freedom modeling for air-breathing hypersonic vehicles," in *Proc. 5th IFAC Conf. Adv. Control Optim. Dyn. Syst. (ACODS)*, Hyderabad, India, 2018, pp. 492–497.
[3] G. Wu, X. Meng, and F. Wang, "Improved nonlinear dynamic inversion control for a flexible air-breathing hypersonic vehicle," *Aerosp. Sci. Technol.*, vol. 78, pp. 734–743, Jul. 2018.
[4] Q. Hu, Y. Meng, C. Wang, and Y. Zhang, "Adaptive backstepping control for air-breathing hypersonic vehicles with input nonlinearities," *Aerosp. Sci. Technol.*, vol. 73, pp. 289–299, Feb. 2018.
[5] H. Wu, "Adaptive robust stabilisation of uncertain nonlinear dynamical systems: An improved backstepping approach," *Int. J. Control*, vol. 91, no. 1, pp. 114–131, 2018.
[6] H. Wu, "Adaptive robust output tracking of uncertain strict-feedback nonlinear time-delay systems via control schemes with simple structure," *Int. J. Syst. Sci.*, vol. 48, no. 12, pp. 2669–2681, 2017.
[7] Y. Cheng, B. Xu, F. Wu, X. Hu, and R. Hong, "HOSM observer based robust adaptive hypersonic flight control using composite learning," *Neurocomputing*, vol. 295, pp. 98–107, Jun. 2018.
[8] J. Wang, Q. Zong, R. Su, and B. Tian, "Continuous high order sliding mode controller design for a flexible air-breathing hypersonic vehicle," *ISA Trans.*, vol. 53, no. 3, pp. 690–698, May 2014.
[9] Y. Wang, M. Chen, Q. Wu, and J. Zhang, "Fuzzy adaptive non-affine attitude tracking control for a generic hypersonic flight vehicle," *Aerosp. Sci. Technol.*, vol. 80, pp. 56–66, Sep. 2018.
[10] X. Bu, G. He, and K. Wang, "Tracking control of air-breathing hypersonic vehicles with non-affine dynamics via improved neural back-stepping design," *ISA Trans.*, vol. 75, pp. 88–100, Apr. 2018.
[11] X. Bu, "Guaranteeing prescribed performance for air-breathing hypersonic vehicles via an adaptive non-affine tracking controller," *Acta Astron.*, vol. 151, pp. 368–379, Oct. 2018.
[12] X. Su and Y. Jia, "Self-scheduled robust decoupling control with H∞ performance of hypersonic vehicles," *Syst. Control Lett.*, vol. 70, pp. 38–48, Aug. 2014.
[13] H.-N. Wu, Z.-Y. Liu, and L. Guo, "Robust L_∞-gain fuzzy disturbance observer-based control design with adaptive bounding for a hypersonic vehicle," *IEEE Trans. Fuzzy Syst.*, vol. 22, no. 6, pp. 1401–1412, Dec. 2014.
[14] H.-N. Wu, S. Feng, Z.-Y. Liu, and L. Guo, "Disturbance observer based robust mixed H_2/H_∞ fuzzy tracking control for hypersonic vehicles," *Fuzzy Set. Syst.*, vol. 306, pp. 118–136, Jan. 2017.
[15] M. Gao and J. Yao, "Finite-time H_∞ adaptive attitude fault-tolerant control for reentry vehicle involving control delay," *Aerosp. Sci. Technol.*, vol. 79, pp. 246–254, Aug. 2018.
[16] X.-H. Zhao, Y. Sun, G.-L. Zhao, and J.-L. Fan, "μ-Synthesis robust controller design for the supercavitating vehicle based on the BTT strategy," *Ocean Eng.*, vol. 88, pp. 280–288, Sep. 2014.
[17] M. Zhu, X. Wang, Z. Dan, S. Zhang, and X. Pei, "Two freedom linear parameter varying μ synthesis control for flight environment testbed," *Chin. J. Aeronaut.*, vol. 32, no. 5, pp. 1204–1214, 2019. doi: 10.1016/j.cja.2019.01.017.
[18] M. Martinino, J. Bordeneuve-Guibé, and V. Morio, "Adaptive augmentation of an optimal baseline controller for a hypersonic vehicle," in *Proc. Annu. Amer. Control Conf. (ACC)*, Milwaukee, WI, USA, Jun. 2018, pp. 4068–4074.
[19] V. Natarajan and J. Bentsman, "Adaptive projection-based observers and L_1 adaptive controllers for infinite-dimensional systems with full-state measurement," *IEEE Trans. Autom. Control*, vol. 59, no. 3, pp. 585–598, Mar. 2014.
[20] H. Jafarnejadsani, H. Lee, and N. Hovakimyan, "L_1 adaptive sampled-data control for uncertain multi-input multi-output systems," *Automatica*, vol. 103, pp. 346–353, May 2019.
[21] C. Han, Z. Liu, and J. Yi, "Immersion and invariance adaptive control with σ-modification for uncertain nonlinear systems," *J. Frankl. Inst.*, vol. 355, pp. 2091–2111, Mar. 2018.
[22] Z. Liu, X. Tan, R. Yuan, G. Fan, and J. Yi, "Immersion and invariance-based output feedback control of air-breathing hypersonic vehicles," *IEEE Trans. Autom. Sci. Eng.*, vol. 13, no. 1, pp. 394–402, Jan. 2016.
[23] L. Hu, R. Li, T. Xue, and Y. Liu, "Neuro-adaptive tracking control of a hypersonic flight vehicle with uncertainties using reinforcement synthesis," *Neurocomputing*, vol. 285, pp. 141–153, Apr. 2018. doi: 10.1016/j.neucom.2018.01.031.
[24] Y. Liu, Z. Pu, and J. Yi, "Observer-based robust adaptive T2 fuzzy tracking control for flexible air-breathing hypersonic vehicles," *IET Control Theory Appl.*, vol. 12, no. 8, pp. 1036–1045, May 2018.
[25] L. Fiorentini, A. Serrani, M. A. Bolender, and D. B. Doman, "Nonlinear robust adaptive control of flexible air-breathing hypersonic vehicles," *J. Guid. Control Dyn.*, vol. 32, no. 2, pp. 402–417, 2009.
[26] B. Xu, S. Wang, and D. Gao, "Parameter estimation based control of hypersonic aircraft with magnitude constraints on states and actuators," in *Proc. Int. Conf. Unmanned Aircr. Syst. (ICUAS)*, Atlanta, GA, USA, May 2013, pp. 875–880.
[27] B. Xu, X. Huang, D. Wang, and F. Sun, "Dynamic surface control of constrained hypersonic flight models with parameter estimation and actuator compensation," *Asian J. Control*, vol. 16, no. 1, pp. 162–174, 2014.
[28] Z. Cai, M. S. de Queiroz, and D. M. Dawson, "A sufficiently smooth projection operator," *IEEE Trans. Autom. Control*, vol. 51, no. 1, pp. 135–139, Jan. 2006.
[29] J. T. Parker, A. Serrani, S. Yurkovich, M. A. Bolender, and D. B. Doman, "Control-oriented modeling of an air-breathing hypersonic vehicle," *J. Guid., Control, Dyn.*, vol. 33, no. 3, pp. 856–869, 2007.
[30] M. A. Bolender and D. B. Doman, "Nonlinear longitudinal dynamical model of an air-breathing hypersonic vehicle," *J. Spacecraft Rockets*, vol. 44, no. 2, pp. 374–387, 2007.
[31] L. Fiorentini, "Nonlinear adaptive controller design for air-breathing hypersonic vehicles," Ph.D. dissertation, Dept. Elect. Comput. Eng., Ohio State Univ., Columbus, OH, USA, 2010.
[32] B. Xu, D. Gao, and S. Wang, "Adaptive neural control based on HGO for hypersonic flight vehicles," *Sci. China Inf. Sci.*, vol. 54, no. 3, pp. 511–520, Mar. 2011.
[33] M. Polycarpou, J. Farrell, and M. Sharma, "Robust on-line approximation control of uncertain nonlinear systems subject to constraints," in *Proc. 9th IEEE Int. Conf. Eng. Complex Comput. Syst.*, Florence, Italy, Apr. 2004, pp. 66–74.
[34] G. Mattei and S. Monaco, "Nonlinear autopilot design for an asymmetric missile using robust backstepping control," *J. Guid. Control Dyn.*, vol. 37, no. 5, pp. 1462–1476, 2014.

SHILI TAN was born in 1991. He received the B.S. degree in weapon system and launching engineering from Air Force Engineering University (AFEU), Xi'an, China, in 2014. He is currently pursuing the Ph.D. degree in control science and engineering with the Air and Missile Defense College, Air Force Engineering University. His research interests are modeling, trajectory optimization, and nonlinear control of hypersonic missiles.

JIONG LI was born in 1979. He received the B.S., M.S., and Ph.D. degrees from the Air Force Engineering University (AFEU), Xi'an, China, in 2000, 2003, and 2007, respectively. He is currently an Associate Professor and a Supervisor for the master's degree at the Air and Missile Defense College, Air Force Engineering University, Xi'an. He is the author of four books and more than 90 articles. His research interests include the guidance, control, and simulation of the hypersonic interceptor.

HUMIN LEI was born in 1960. He received the M.S. and Ph.D. degrees in navigation guidance and control from the School of Astronautics, Northwestern Polytechnical University (NWPU), Xi'an, China, in 1989 and 1999, respectively. He was a Postdoctoral Fellow in control science and engineering with Xi'an Jiaotong University (XJTU). He is currently a Professor and a Supervisor of doctors with the Air and Missile Defense College, Air Force Engineering University (AFEU), Xi'an. He is the author of two books, there patents, and more than 150 articles. His current research interests include the field of advanced guidance law design, hypersonic vehicle controller design, and hypersonic interception strategy.